Powered Transtibial Prosthetic Device Control System Design, Implementation and Testing

Jinming Sun
Marquette University

POWERED TRANSTIBIAL PROSTHETIC DEVICE CONTROL SYSTEM DESIGN, IMPLEMENTATION AND TESTING

by

Jinming Sun, B.S.

A Thesis Submitted to the Faculty of the Graduate School,
Marquette University,
in Partial Fulfillment of the Requirements for
the Degree of Master of Science

Milwaukee, Wisconsin

December 2012

ABSTRACT

CONTROL ALGORITHM DESIGN AND SYSTEM IMPLEMENTATION OF A POWERED TRANSITIAL PROSTHETIC DEVICE

Jinming Sun, B.S.

Marquette University, 2012

A powered lower limb prosthesis, which consists of a four bar mechanism, a torsional spring and a brushed DC motor, was previously designed and fabricated. To regulate the motor power input, a two level controller was proposed and built. The control algorithm includes a higher level finite state controller and lower level PID controllers.

To implement the control system, a digital signal processor (DSP) control board and MATLAB Simulink were used to realize the higher level control and a DC motor controller was used to realize the lower level PID control. Sensors were selected to provide the required feedback. The entire control system was implemented on a convenient to carry backpack.

Amputee subject testing was performed to obtain some experimental verification of the design. The results showed that the control system performed consistently with the designed control algorithm and did assist in the amputee's walking. Compared to a currently available powered prosthesis, this control is simple in structure and able to mimic the nonlinear behavior of the ankle closely.

ACKNOWLEDGEMENTS

Jinming Sun, B.S.

I would first and foremost like to thank Dr. Philip A. Voglewede for providing me with advice. This work could not have been completed without his support and guidance. In addition, I would like to thank Dr. Kevin Craig and Dr. Joseph Schimmels for their helpful comments and suggestions. A special thanks goes to Brian Slaboch for the numerous discussions I had with him and his helpful advice. I would also like to thank Bryan Bergelin for the mechanism design which made my thesis possible. Finally, the I would like to thank my family and friends for their encouragement and guidance.

TABLE OF CONTENTS

ACKNOWLEDGEMENTS . . . . . **i**

TABLE OF CONTENTS . . . . . **ii**

LIST OF FIGURES . . . . . **iv**

CHAPTER 1 Introduction **1**
1.1 Motivation 1
1.2 Related Work 2
1.2.1 Ossur Proprio Foot with Evo 2
1.2.2 SPARKY from Arizona State University 4
1.2.3 Vanderbilt Powered Knee and Ankle Prosthesis 7
1.2.4 BioM - MIT Powered Ankle-Foot Prosthesis 10
1.3 Summary 14

CHAPTER 2 Previous Work **16**
2.1 Mechanical Design 16
2.2 Four-Bar Mechanism Optimization 18
2.3 Components Selection and Prototype Fabrication 19
2.3.1 Active and Passive Components 19
2.3.2 Prototype Fabrication and Bench Testing 20

CHAPTER 3 Overall Control Algorithm **22**
3.1 Dynamics of Human Gait 22
3.2 Proposed Control Algorithm 23
3.3 Higher Level Controller Schematic 25
3.4 Lower Level PID Controllers 28
3.4.1 PI Moment Controller 28
3.4.2 PID Position Controller 30
3.5 Conclusion 31

CHAPTER 4 Control System Realization **32**
4.1 Hardware Configuration 32
4.1.1 Higher and Lower Level Controller Hardware 33
4.1.2 Sensors 34
4.2 Software Programming 36
4.2.1 Higher Level Control Algorithm Programming 36
4.2.2 Lower Level Control Programming 38
4.3 Portable Testing Platform 39
4.4 Conclusion 39

TABLE OF CONTENTS — *Continued*

CHAPTER 5 Dynamic Modeling and Simulation 41
5.1 Assumptions 41
5.2 Four Bar Mechanism Modeling 43
5.2.1 Stance Phase Modeling 44
5.2.2 Swing Phase Modeling 46
5.3 Dynamic Simulation and PID Tuning 47
5.3.1 Stance Phase Simulation 48
5.3.2 Swing Phase Simulation 49
5.4 Robustness Testing of the Dynamic Model 51
5.5 Conclusion 52

CHAPTER 6 Bench Testing and Amputee Subject Testing 53
6.1 Moment Bench Testing 53
6.1.1 Bench Testing Configuration 54
6.1.2 Bench Testing Results and Interpretation 54
6.2 Amputee Subject Testing Method 55
6.3 Amputee Subject Testing Results and Discussion 56
6.3.1 Result Analysis between Trials Wearing Powered Prosthesis 57
6.3.2 Result Analysis between the Prosthesis, Natural Leg and Winter's Data 59
6.3.3 Result Analysis between the Powered Prosthesis and the Passive Prosthesis 61
6.4 Conclusion 62

CHAPTER 7 Conclusion and Future Work 64
7.1 Conclusion 64
7.2 Future Work 67
7.2.1 Improve the Efficiency 67
7.2.2 Reselection of the Motor 67
7.2.3 More Sophisticated Higher Level Control Algorithm 68
7.2.4 More Advanced Lower Level Controller 68
7.2.5 Redesign the Portable Platform 68

REFERENCES 69

APPENDIX A Kinematics Derivation of the Four-Bar Mechanism 73

APPENDIX B Simulink and Stateflow Control Program 78

APPENDIX C Amputee Subject Testing Data 84

LIST OF FIGURES

1.1 Össur Proprio Foot with EVO Design [1] 2
1.2 The "Sense-Think-Act" Control Strategy of the Össur Proprio Foot with EVO Design [1] 3
1.3 SPARKY CAD Model and Prototype [2] 5
1.4 This diagram illustrates the flow of energy from the battery to the user for the robotic tendon model [3] 6
1.5 The Self-Contained Powered Knee and Ankle Prosthesis from Vanderbilt University [4] 8
1.6 A Three Level Control Algorithm Is Utilized in the Transfemoral Prosthesis [5] 9
1.7 Mechanical Model of the MIT Powered Ankle-Foot Prosthesis [6] 11
1.8 BioM: The MIT Powered Ankle-Foot Prosthesis [6] 12
1.9 Overall Control Algorithm Flow Diagram of the MIT Powered Ankle-Foot Prosthesis [6] 13
2.1 The Nonlinear Profile of the Ankle Joint Moment in One Gait Cycle [7] . 17
2.2 The Sketch of the Mechanism Design Concept 17
2.3 The Prototype of the Designed Prosthesis 20
2.4 The Results of the Bench Testing of the Transtibial Prosthesis with the Active Components Turned Off 21
3.1 The Proposed Overall Control Algorithm 24
3.2 The Proposed Finite State Machine Working Schematic 27
3.3 The Fitted Curve Compared to the Reference Moment 28
3.4 The Sketch of the Mechanism Design Concept 30
4.1 The Hardware System Configuration 32
4.2 Force Sensing Resistors 34
4.3 Accompanying Electric Circuits for the FSR Sensors 35
4.4 Complete Higher Level Control Flow Graph Considering Different Situations 37
4.5 PI Moment Control Block Diagram 38
4.6 PID Position Control Block Diagram 38
4.7 The Backpack with All the Hardware Components 38
5.1 SimMechanics Model of the Prosthesis during Stance Phase 45
5.2 The Stance Phase Prosthesis Model Built in Fig. 5.1 45
5.3 SimMechanics Model of the Prosthesis during Swing Phase 46
5.4 The Swing Phase Prosthesis Model Built in Fig. 5.3 47
5.5 The Entire Stance Phase Simulation Model 48
5.6 The Simulation Result of the Ankle Moment during Stance Phase 48
5.7 Decomposed Simulation Result of the Ankle Moment during Stance Phase 49
5.8 The Entire Swing Phase Simulation Model 50
5.9 The Simulation Result of Joint C Position during Swing Phase 50
5.10 Stance Phase Simulation with White Noise 51

LIST OF FIGURES — *Continued*

5.11 Swing Phase Simulation with White Noise 51
6.1 Moment Bench Testing Configuration 54
6.2 The Results of the Moment Bench Testing 55
6.3 The Ankle Angle Comparison between the Three Trials of the Powered Prosthesis 57
6.4 The Ankle Moment Comparison between the Three Trials of the Powered Prosthesis 58
6.5 The Ankle Angle Comparison between the Powered Prosthesis, the Natural Leg and Winter's Data 59
6.6 The Ankle Moment Comparison between the Powered Prosthesis, the Natural Leg and Winter's Data 59
6.7 The Ankle Angle Comparison between the Powered Prosthesis and the Passive Prosthesis 61
6.8 The Ankle Moment Comparison between the Powered Prosthesis and the Passive Prosthesis 61
A.1 The Sketch of the Four-Bar Mechanism Kinematics 73
B.1 Overall Control Program Built in Simulink and Stateflow Toolbox 79
B.2 Higher Level Control Program Using Stateflow Toolbox 80
B.3 Lower Level PI Moment Control Program 81
B.4 Lower Level PID Position Control Program 82
B.5 FSR Simulink Subsystem 83
C.1 The GRF Comparison between the Three Trials of the Powered Prosthesis 84
C.2 The Ankle Power Comparison between the Three Trials of the Powered Prosthesis 85
C.3 The GRF Comparison between the Powered Prosthesis, the Natural Leg and Winter's Data 86
C.4 The Ankle Power Comparison between the Powered Prosthesis, the Natural Leg and Winter's Data 87
C.5 The GRF Comparison between the Powered Prosthesis and the Passive Prosthesis 88
C.6 The Ankle Power Comparison between the Powered Prosthesis and the Passive Prosthesis 89

CHAPTER 1

Introduction

1.1 Motivation

Transtibial amputations, also known as "below knee" amputations, are among the most frequently performed major limb amputations. Statistical data shows that about half of all major lower-limb amputations are transtibial [8] with about 40,000 transtibial amputation surgeries performed every year in the U.S [9]. Designing a functional and comfortable transtibial prosthesis is critical to help transtibial amputees with their daily life.

Recent studies show that, during an able-bodied person's walking, the ankle joint produces more energy than it actually absorbs [10]. It would be beneficial if external power could be provided to the prosthetic device, otherwise, if the prosthetic device is passive, the prothesis users have to use more energy. This results in abnormal gait, more energy expenditure and less energy efficiency [11].

However, most of the current commercially available transtibial prosthesis are passive, which means they basically function as a combination of springs and dampers [12]. As the power of the computers becoming stronger and capacity and size of the batteries becomes better for portable use, the future of the transtibial prosthesis lies ahead in those which can provide active power.

In the light of this idea, a powered transtibial prosthesis was designed and fabricated in previous work [13]. A four-bar mechanism was utilized to mimic the nonlinear behavior of the ankle; a torsional spring was used to reserve the energy during the early stage of a gait cycle and release that energy to help the amputee push-off during the latter stage. More importantly, a brushed DC motor is connected with the four-bar mechanism to provide the extra required energy. Therefore, there comes the need to regulate the power the motor generates. The objective is to make the total moment at the prosthetic ankle consistent with that of an able-bodied person's ankle. **The purpose of this thesis is to design and**

Figure 1.1: Össur Proprio Foot with EVO Design [1]

implement a control system to achieve this objective and perform amputee subject testing to evaluate the functionality of the mechanism designed in previous work and its control system.

1.2 Related Work

Several groups, both in industry and academia, have made state-of-the-art contributions to the development of the powered transtibial prostheses. Some of them are already commercially available, while the other groups have successfully built their prototype and performed human subject testing. Since the majority of the work in this thesis is to design and implement a control system, the literature review is going to concentrate on how the control systems were designed.

1.2.1 Össur Proprio Foot with Evo

The Proprio Foot from Össur is the first active transtibial prosthesis that is commercially available. The latest iteration of this prosthesis is called Proprio Foot with Evo as shown in Fig. 1.1. However, it is not considered to be a fully powered transtibial prosthesis because its active components are only used to position the ankle angle for larger swing leg clearance. It cannot provide any extra energy when the foot is pushed off from the ground.

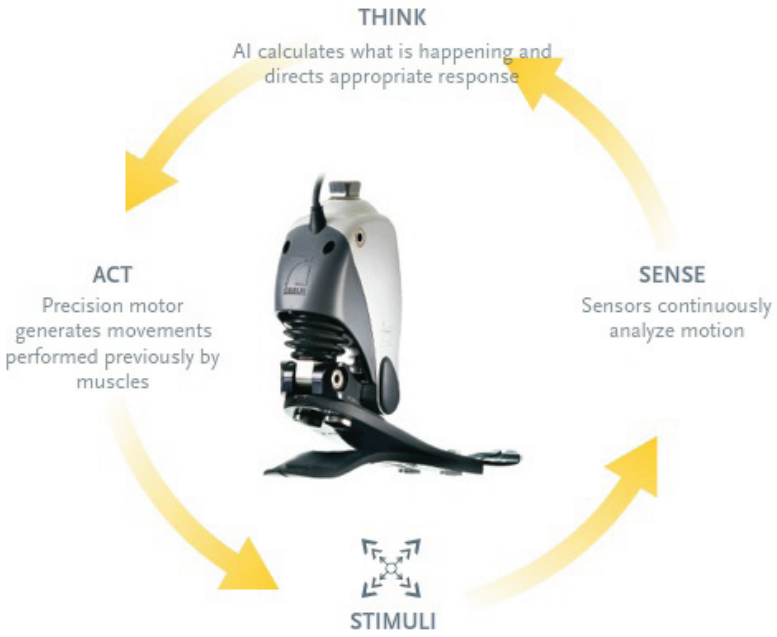

Figure 1.2: The "Sense-Think-Act" Control Strategy of the Össur Proprio Foot with EVO Design [1]

Mechanical Design

The core design concept of this prosthesis is based on Flex-Foot technology, which incorporates lightweight, yet very strong carbon fiber that is cured and layered in processes which are similar to those used in aerospace industry [1].

The Flex-Foot technology is a prosthesis technology which integrates a shock absorption system into the prostheses. It utilizes a carbon fiber compression spring and two telescoping tubes which can move vertically up to one inch. This design can cushion the impact of heel strike to the amputee's residual limb, allowing the users to land on their prosthesis with better comfort.

Control Algorithm and System Configuration

The active components built on top of the Flex-Foot include sensors, a linear spring, a transmission and a precision stepper motor. A logic controller, which uses a control strategy called "Sense-Think-Act", incorporates these components and enables appropriate responses to variations in ground surface and activity. This controller is a typical feedback control algorithm which collects the feedback information from the sensors, processes the information using a processor and

execute the command using the actuators.

The sensor system includes several accelerometers and an angle sensor. They sample ankle motion over 1,000 times per second during a prosthesis user's walking, identifying specific ankle motion events such as heel strike and push off. Motion is analyzed with gait pattern recognition algorithms detecting if a user is doing normal walking, stair climbing, stationary standing or seating. These data is fed back into the logic microcontroller for further processing.

Based on what type of motion the user is doing, a logic microcontroller determines the most appropriate move. For example, if it determines that the user is climbing stairs, during the swing phase, it will adjust the prosthesis angle to be aligned with the slope. It always learns from the user's previous stride to adapt for the next step. Therefore, it will have some difficulties on the transition between different types of motion. For example, if a user is switching from level walking to stair climbing, for the first step of the climbing, the controller will not recognize the user's intent and make it harder to for the user to climb the first step.

The actuator movements are generated by a stepper motor. By adjusting the position of the linear spring, the movements that can be achieved include the ankle dorsiflexsion as the leg swings forward and the adjustment of ankle angle on varying terrain and heel height when changing shoes.

1.2.2 SPARKY from Arizona State University

The "SPARKY" project, which stands for Spring Ankle with Regenerative Kinetics, is a transtibial prosthesis designed by a group headed by Dr. Thomas Sugar at Arizona State University. So far, there have been three iterations of this prosthesis which are respectively named SPARKY 1, 2 and 3 [3, 14–16]. Human subject testing has been successfully performed using this prosthesis, and the results showed that it is capable of reproducing the power and motion profile of an able-bodied person's ankle.

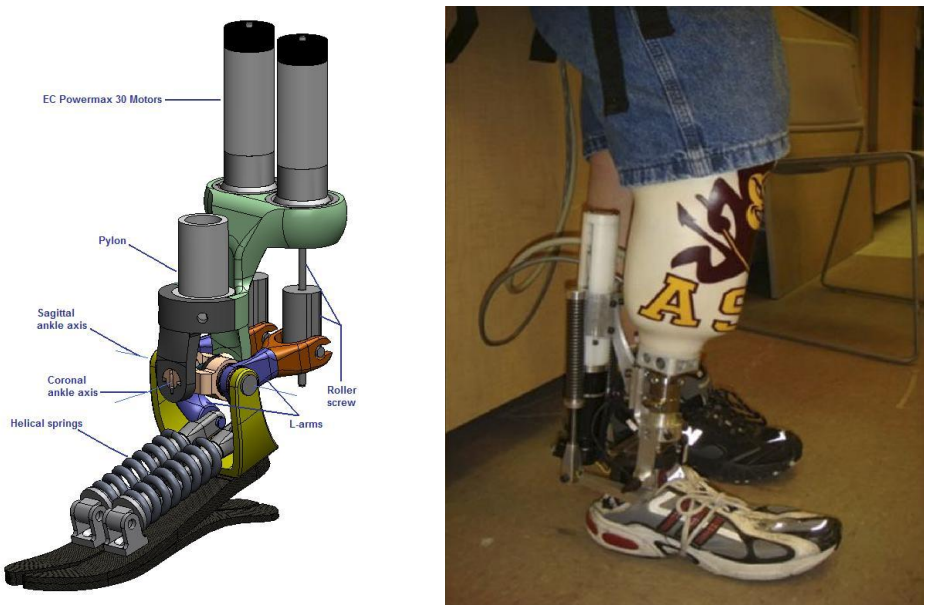

Figure 1.3: SPARKY CAD Model and Prototype [2]

Mechanical Design

The major components of the SPARKY include a Össur LP Vari-Flex foot, a robotic tendon, a high output brushless DC motor. The robotic tendon mechanism has two helical springs, a lever arm and a roller screw/ball screw interchangeable transmission. A CAD model and a picture of the prototype are shown in Fig. 1.3.

In this simple series model, the LP Vari-Flex foot is connected in series with the robotic tendon springs, therefore, the moment in the foot is the same as the moment in the robotic tendon. The motor is also connected in series with the spring to adjust the position of the springs so that the moment of the robotic tendon matches that of the able-bodied moment data [3].

The first two iterations of this prosthesis are limited to active motion only in the saggital plane. The latest version, SPARKY 3, added another degree-of-freedom along the coronal plane by adding a second motor and two joints without increasing the overall volume [2].

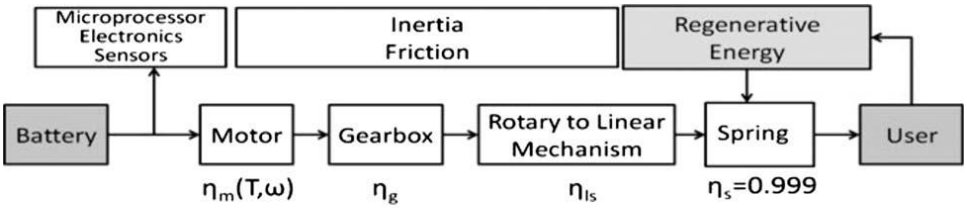

Figure 1.4: This diagram illustrates the flow of energy from the battery to the user for the robotic tendon model [3]

Control Algorithm

Its control system, as described in detail in [15, 16], has a predetermined gait pattern, which is based on able-bodied people's gait data from Whittle [17] and kinetic analysis. The reference profile is expressed as a time-based function embedded in the controller, which drives the motor controller and thus the system. Gait is initiated at heel strike with the activation of an optical switch embedded in the heel of the LP Veri-Flex Foot. As the patient initiates gait, the motor drives the lead screw nut through a predetermined pattern with closed loop feedback. The ankle, however, is not forced to follow the specific pattern because the compliant spring is between the motor and the amputee, safely absorbing environmental irregularities such as a rock under foot or the user's unexpected behavior [14]. The diagram in Fig. 1.4 illustrates the flow of power and energy from the battery to the users.

Two other state-of-the-art control algorithms, which are named "Tibia Based Controller Theory" and "Dynamic Pace Control" respectively, are presented by Holgate et al. [18, 19]. Simulation and preliminary testing were performed on these two algorithms. Results showed that they have certain advantages and disadvantages over the convention prosthesis control method. They are still in conceptual stage and are not used in the SPARKY prosthesis.

Control System Implementation

To implement this control system, Real Time Workshop and Simulink from Mathworks were utilized. The Simulink model is compiled onto the embedded target PC running the xPC Target Operating System. The sensors include an encoder at

the motor, an encoder at the ankle joint and an optical switch embedded at the heel. Advantech's 650 MHz PC-104 with 512 MB on-board memory was selected to run the system. This is a widely used computing system when implementing a portable device. A multifunctional I/O board from Sensoray Co. is connected to the PC 104 via an ISA bus to control the motor with encoder feedback [14].

Human subjects testing results showed that, with the motor connected in series with the robotic tendon, the output power of the prosthesis is consistently 3 to 4 times larger than the input power from the motor. The maximum power amplification reaches 6 during the testing phase. The total output power reaches 270 W at push-off which suggests enough power is generated comparing with 250 W for able-bodied people's normal walking [14].

1.2.3 Vanderbilt Powered Knee and Ankle Prosthesis

Several iterations of a powered knee and ankle transfemoral prosthesis have been designed in a group led by Dr. Michael Goldfarb at Vanderbilt University. It is different from the previous mentioned prosthesis in that it is a prosthesis for both the knee and the ankle. The first prototype is a tethered prosthesis powered by pneumatic actuators [20]. The latest prototype is a self-contained active knee and ankle prosthesis, which is actuated electrically by using a lithium polymer battery.

Mechanical Design

The major components of the Vanderbilt prosthesis include a customized foot, a spring which is incorporated inside the ankle, a slider-crank and two actuators. The prototype is shown in Fig. 1.5.

The actuation for the prosthesis is provided by two motor-driven ball screws which drive the knee and the ankle, respectively, through the slider-crank. Each actuation unit has a motor which is connected to a ball screw via helical shaft coupling. The ankle incorporates a spring, which is in parallel with the ball screw. The purpose of this spring is to bias the motor's axial force output toward ankle pantarflextion, and to supplement power output during ankle push off. There is a

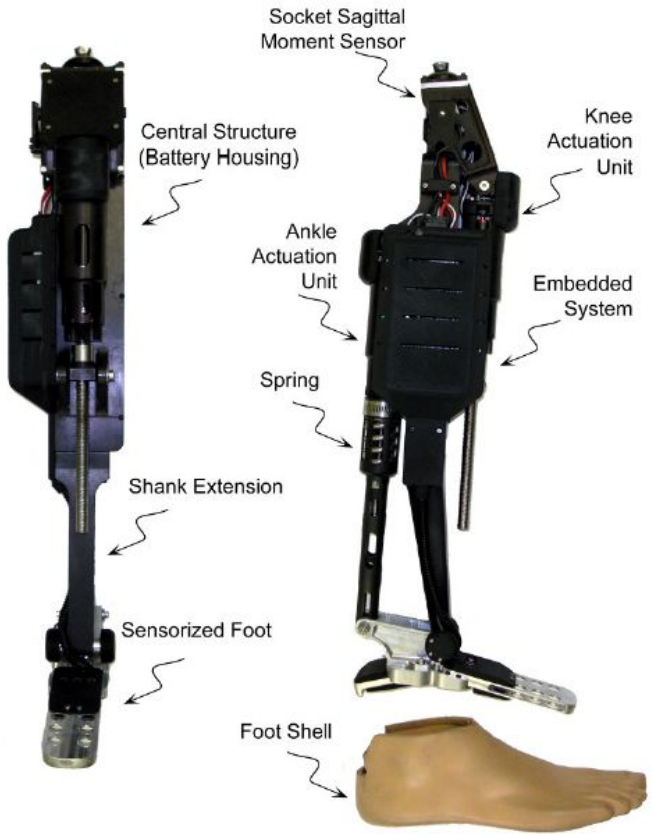

Figure 1.5: The Self-Contained Powered Knee and Ankle Prosthesis from Vanderbilt University [4]

uniaxial load cell positioned in series with each actuation unit to control the motor and ball screw unit. The ankle joint connects to a custom foot design which incorporates strain gauges to measure the ground reaction forces on the foot and the heel.

The total mass of the self-contained device is 4.2kg, which is within an acceptable range for transfemoral prostheses, and comparable to a normal limb segment [5].

Control Algorithm

The control algorithm of the prosthesis is a three-level controller as shown in Fig. 1.6. The high-level controller, which is called the intent recognizer, indicates the amputee's intent according to what interaction the amputee has with the prosthesis, then switches the middle-level controllers between level walking mode

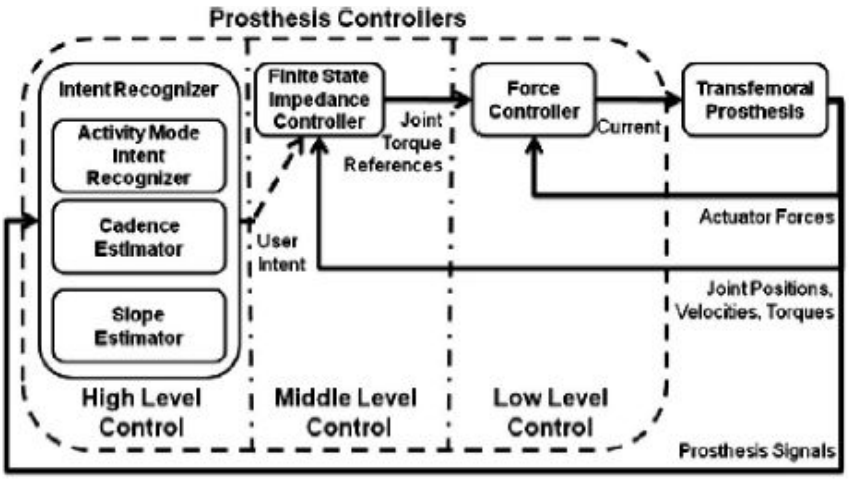

Figure 1.6: A Three Level Control Algorithm Is Utilized in the Transfemoral Prosthesis [5]

and standing mode accordingly. Intent recognition is accomplished by first generating a database containing sensor data from different activity modes and training a pattern recognizer that switches between two activity modes, which are walking mode and standing mode, in real time.

The middle-level controller is developed for each activity mode using an impedance control method. The impedance control uses an impedance based approach to generate joint moment reference. The joint moment reference for each mode are governed by separate controllers, which modulate the joint impedance according to the phase of the gait. Each of the two modes is further divided into several phases. Every phase has different reference input. The level walking mode is described by five phases, three of which are stance phases and two of which are swing phases. The standing mode is described by two phases, which are a weight-bearing phase and a nonweight-bearing phase [5].

The low-level controllers are the closed-loop joint moment controllers, which compensate for the transmission dynamics of the ball screw, and thus, enable tracking of the knee and ankle joint moment reference input.

Control System Implementation

As mentioned above, the actuating system includes two motors connected with two motor driven ball screws that drive the knee and ankle joints respectively.

The sensing system includes the moment sensors measuring the sagittal plane moment at the knee and ankle joint of the prosthesis and the force sensors measuring the force between the prosthesis and the ground. The sagittal plane moment sensor incorporates strain gauges that measure the strains generated by the sagittal plane moment. A custom foot was designed to measure the strains that resulting from the ground reaction force at the ball and the heel of the foot. By measuring the strains, the moment and ground reaction force can be calculated using the strain-stress relationship.

The main computational element of the embedded system is an PIC32 microcontroller with 512kB flash memory and 32kB RAM. The microcontroller is programmed in C using MPLAB IDE and MP32C Compiler. During the testing, the prosthesis can be controlled by a laptop running MATLAB Simulink RealTime Workshop. The microcontroller sends pulse-width modulation (PWM) reference signals to two DC motor drivers, which drive the motors [5].

1.2.4 BioM - MIT Powered Ankle-Foot Prosthesis

Designed and built by the MIT Media Lab, which is led by Dr. Hugh Herr, the MIT powered transtibial prosthesis, named BioM, is the most advanced prosthesis in the research field of transtibial prosthesis [6, 21, 22]. This prosthesis has successfully become commercially available for testing in recent years by iWalk, LLC.

Mechanical Design

The mechanical model of this prosthesis is shown in Fig. 1.7. Its major components include a Össur Flex-Foot, a unidirectional parallel spring, a series spring, a powered drive train and a brushless motor with its transmission.

The ankle joint is a ball bearing which connects the lower Flex-Foot to an upper leg shank structure topped with a prosthetic fixture to attach to the prosthesis socket. The Flex-Foot is efficient in minimizing the ground contact shock during the heel strike. A unidirectional parallel spring engages when the ankle and

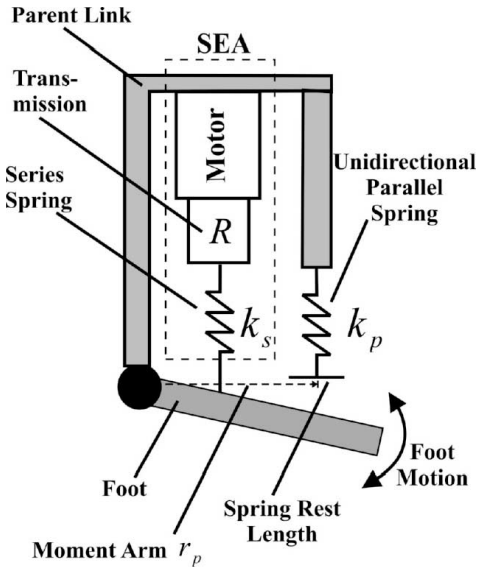

Figure 1.7: Mechanical Model of the MIT Powered Ankle-Foot Prosthesis [6]

the foot are perpendicular to each other. It acts in parallel to a powered drive train to provide the passive function of an Archilles tendon. The motor is mounted at the upper leg shank end. It acts through the transmission on the series spring.

The series spring is a Kevlar-composite material leaf spring, which connects the foot to the ball nut with a moment arm. The effective rotary stiffness due to the series spring changes depending on if the foot is in plantar-flexion or dorsiflexion. The drive train and the series spring together comprise a series-elastic actuator called "SEA" which is the major design concept of this prosthesis. The prototype of this prosthesis is shown in Fig. 1.8.

One of the biggest challenge in the design of transtibial prosthesis is how to mimic the nonlinear behavior of the human ankle. The MIT prosthesis uses a unidirectional parallel spring and a series spring to solve this issue. In the mechanical design of this thesis, a four-bar mechanism combined with a torsional spring is utilized to achieve the same function.

Control Algorithm

The control system of the MIT powered transtibial prosthesis includes a finite-state controller and a set of low-level servo controllers. The overall flow diagram of the control system is shown in Fig. 1.9. The low-level servo controllers

Figure 1.8: BioM: The MIT Powered Ankle-Foot Prosthesis [6]

were used to support basic human ankle functions, such as providing the desired position or the desired moment. The high level finite state machine was used to manage and determine the transitions among the low-level servo controllers. The finite state machine comprised a state identification algorithm and a state control. The state identification was to identify the current state of the prosthesis; the state control was used to execute the predefined procedure for a given state. Local sensing information, including the ankle angle, ankle torque, and foot contact information, were used for the state detection and transition.

The low-level servo controllers includes a PD torque controller, a impedance controller and a PD position controller. The finite state machine divides one cycle of gait into stance phase and swing. The stance phase is further divided into three states, namely controlled plantar-flexion (CP), controlled dorsiflexion (CD) and powered plantar-flexion (PP). During the CP and CD states, the prosthesis works under the impedance control mode and outputs a joint stiffness. During the PP state, the prosthesis works under the PD torque controller and outputs a constant offset torque. The swing phase is also divided into three states, namely SW1, SW2, SW3. When the prosthesis is in SW1 and SW2 states, it works under the PD position mode and moves toward a predefined position. During the SW3 state, the controller resets the system to the impedance control mode [6].

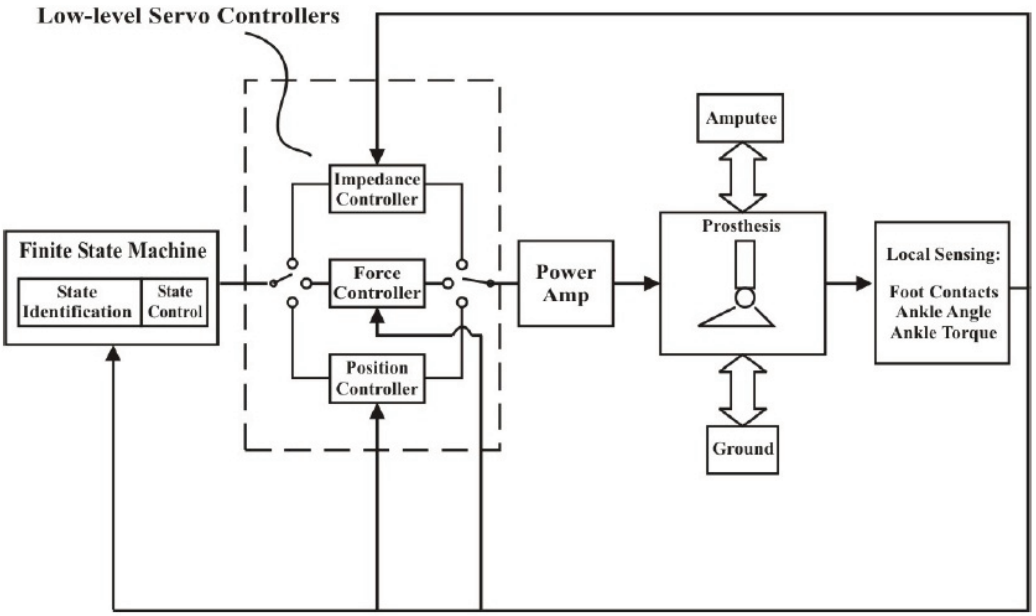

Figure 1.9: Overall Control Algorithm Flow Diagram of the MIT Powered Ankle-Foot Prosthesis [6]

In their latest iteration of the controller design, an adaptive muscle-reflex controller was utilized. The controller determines the appropriate torque using a neuromuscular model of the human ankle-foot complex. In this model, a hinge joint, which represents the human ankle, is actuated by two competing virtual actuators, which include a unidirectional plantar flexor and a dorsiflexor. The former one is a Hill-type muscle model and the latter one is a bi-directional PD position controller. Depending on the gait phase, one or the other, or both of them produce torques at the ankle joint [23].

System Implementation

The high-level control and communication for the ankle-foot prosthesis are provided by a single-chip, 16-bit digital signal processor (DSP) from Microchip Technology Inc. A second identical DSP microcontroller was used as the low-level dedicated motor controller. All power for the prosthesis was provided by a lithium polymer battery, which is able to provide a day's power requirements including five thousand steps of walking.

The sensing system includes two Hall-effect sensors, one set of strain gauges

Table 1.1: Comparison Between Current Powered Below-Knee Prostheses

	Components to Mimic Nonlinear Ankle Impedance	Actively Provide Power	Multiple Level Controllers
Össur Proprio	No	No	No, only position control
SPARKY	No	Yes	No, following a predetermined pattern
Vanderbilt	A slider crank, a ball screw and a spring	Yes	Yes, three level
BioM	A parallel spring and a series spring	Yes	Yes, two level

and a optical motor encoder. A hall-effect angle sensor at the ankle joint is a primary feedback signal. Another linear Hall-effect sensor is mounted on the main housing to measure the ankle joint angle. Strain gauges located on the series spring permit sensing of the output torque of the motorized drive train, thereby allowing for closed loop torque control of the SEA. The motor itself contains Hall-effect commutation sensors and is fitted with an optical shaft encoder that enables the use of advanced brushless motor control techniques.

1.3 Summary

The previously mentioned prostheses contributed significantly to the development of the mechanical design and control algorithm design to the transtibial prostheses. They are compared in Tab. 1.1 from three perspectives. The mechanical design of the transtibial prosthesis described in this thesis is with a simpler mechanism: a four-bar mechanism and a torsional spring. This mechanism is different from the above mentioned mechanisms in that it can mimic the nonlinear stiffness behavior of the human ankle with respect to time. It is possible to be controlled with respect to time instead of having to be controlled with respect to the angle of the ankle. Therefore, a different control algorithm and system implementation have to be designed for this prosthesis.

In Chapter 2, the previous work of the mechanical design of the prosthesis is briefly described. An optimization was performed to obtain the parameters of this mechanism. A finite element analysis was completed to verify that the mechanism has sufficient strength. The prototype of this prosthesis was fabricated and bench

tested. Test results showed that this prosthesis meets the design requirement. In Chapter 3, the overall control algorithm is illustrated. A two level control algorithm is used. The higher level finite state controller and the lower level PID controllers are described in detail. In Chapter 4, the implementation of the control system is discussed. The hardware, software, the sensors and the power supplies are demonstrated. In Chapter 5, a dynamic model is built using MATLAB Simulink to simulate the dynamic process and adjust the PID gains of the lower level controllers. In Chapter 6, bench testing was first performed to verify that the motor is capable of generating the required moment. Amputee subject testing are conducted in the gait lab to obtain some experimental data to support the proposed design. The testing results are analyzed. In Chapter 7, the conclusion is made and the ideas of the future work are explored.

CHAPTER 2

Previous Work

This work builds upon the previous research of the mechanical design of a new type of transtibial prosthesis. Therefore, an overview of the mechanical design is presented in this chapter. The first iteration of the prototype of this prosthesis was built and tested by Mattos et al. [24]. Bergelin et al. [13] revisited the design, making the prosthesis lighter and its range of motion larger. Several important assumptions were made before designing the prosthesis:

1. The movement of the prosthesis is restricted to the sagittal plane. The movement in the transverse plane and coronal plane is neglected.
2. Only normal level walking pattern is considered since this is the first iteration of prosthesis.
3. The ankle moment and other data from [7] is used as benchmark of this design because of its widespread use as standard gait analysis data.
4. A body mass of 86.4 kg is assumed for calculations and design.
5. Friction in the joints is neglected.

2.1 Mechanical Design

The literature [7, 10, 11] shows that one of the most important aspects in an able-bodied person's walking is that the ankle needs to generate enough moment to propel the body forward during push-off. When an able-bodied person is walking, the moment generated at the ankle is a profile as shown in Fig. 2.1. Four-bar mechanisms are one of the most common mechanisms which can generate nonlinear kinematics in mechanical design. Therefore, a four-bar mechanism is utilized as the key design concept in this prosthesis to mimic the nonlinear behavior of the ankle.

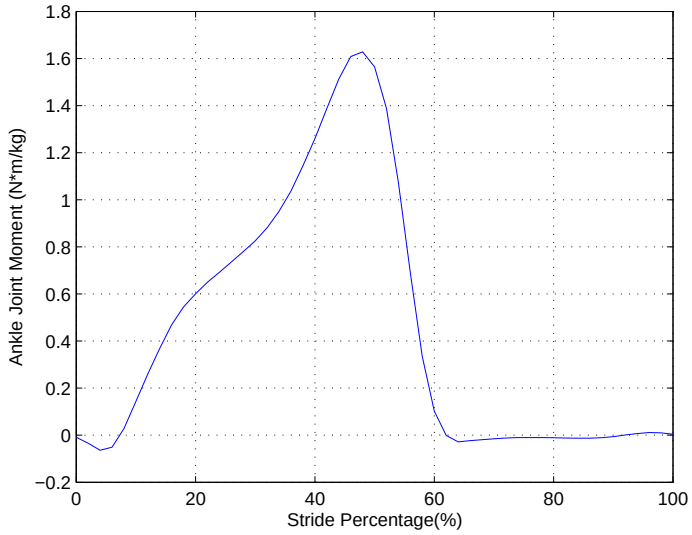

Figure 2.1: The Nonlinear Profile of the Ankle Joint Moment in One Gait Cycle [7]

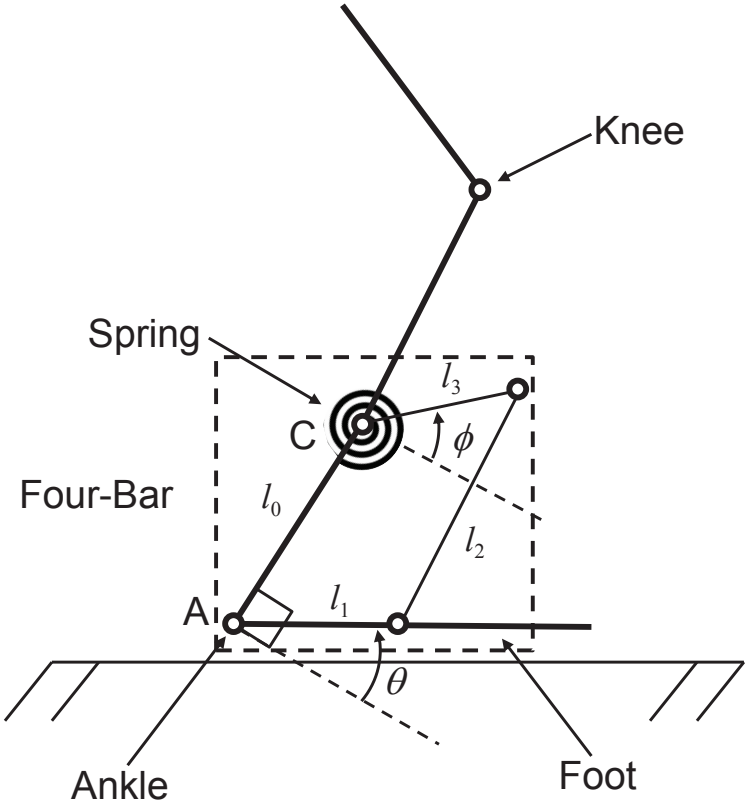

Figure 2.2: The Sketch of the Mechanism Design Concept

A torsional spring is used to store energy during the early stage of the gait cycle and release the energy to help the "push-off" during the later stage.

While the four-bar mechanism and the torsional spring can provide the

majority of the energy, active components are still needed to provide extra energy since the ankle joint produces more energy than it actually absorbs during one gait cycle [10]. A brushed DC motor is added to the mechanism to provide the extra required energy. The sketch of the overall mechanism design concept is shown in Fig. 2.2.

To realize a better mechanism, the optimal lengths of each link of the four-bar mechanism needs to be determined, which can be formulated as a optimization problem. The parameters of the torsional spring also needs to be determined and the active components need to be selected.

2.2 Four-Bar Mechanism Optimization

The optimization of the four-bar mechanism was first developed by Mattos et al. [24] and later revised by Bergelin et al. [13]. The principle of this optimization is that the error between the theoretical ankle moment and the optimized ankle moment plus an energy penalty function should be minimized. The objective function utilized was:

$$\begin{aligned} \min \quad & E = \sum (M_i - M_{\theta_i})^2 + \gamma |b| \\ \text{where} \quad & \gamma = 0.03 \end{aligned} \tag{2.1}$$

where E is the term which should be minimized, M_i is the desired ankle moment from [7] at each datum point i, M_{θ_i} is the optimized moment at the ankle, γ is the multi-objective optimization weighting parameter which was chosen by trial and error to be 0.03 to decrease energy input without affecting the optimized M_{θ_i} significantly and $|b|$ is the damping coefficient, which represents the velocity dependent control input gain.

The optimized results for an assumed 86.4kg amputee are:

$$x_{opt} = \begin{bmatrix} b \\ k \\ M_0 \\ l_0 \\ l_1 \\ l_2 \\ l_3 \end{bmatrix} = \begin{bmatrix} -1.606 \frac{N \cdot m \cdot s}{rad} \\ 26.635 \frac{N \cdot m}{rad} \\ -17.005 N \cdot m \\ 6.000 cm \\ 5.48 cm \\ 9.00 cm \\ 2.00 cm \end{bmatrix} \tag{2.2}$$

where k represents the stiffness of the torsional spring, M_0 represents the preload moment on the torsional spring and $l_0 - l_3$ represent lengths of the four-bar linkage as shown in Fig. 2.2. The result of the objective function penalty was small, which proves that, in theory, this mechanism should be capable of mimicking the nonlinear stiffness behavior of the ankle. The details of this optimization are shown in [13].

2.3 Components Selection and Prototype Fabrication

2.3.1 Active and Passive Components

The selection of the active components is a process of balancing the trade-offs [13]. The more powerful the active components are, normally the more power they consume and the larger and heavier the power-supplies have to be. A brushed DC motor was used to keep the controls simple and the power supply portable. Brushed motors are more efficient, and produce more nominal and stall torque than that of the brushless motors. The power rating of the motor was sacrificed in order to reduce the overall size and weight. The motor that was chosen is a Maxon RE-40 graphite brushed motor. The encoder that was selected is a Maxon HEDL 5540 optical encoder for compatibility with the motor. The motor controller selected was a Maxon EPOS2 50/5 positioning controller, because it is compatibility with the Maxon motor, can work under different modes and easy to use. The selected active components are shown in Tab. 2.1.

The passive components include the transmission gearbox which is connected to the motor, the torsional spring and the four-bar linkage. A customized two stage

Table 2.1: The Selected Active Components

Components	Selected Device
Motor	Maxon RE-40 Brushed DC Motor
Encoder	Maxon HEDL 5540 Optical Encoder
Motor Controller	Maxon EPOS2 50/5 Positioning Controller

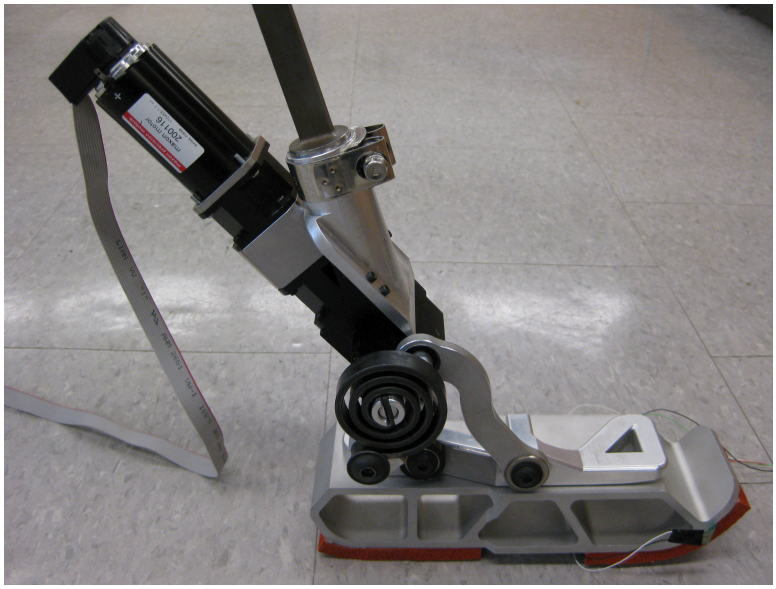

Figure 2.3: The Prototype of the Designed Prosthesis

CGI right-angled gearhead was determined to be the best fit to obtain the desired performance. Its gear ratio is 50:1 and efficiency is about 80%. As mentioned in Section 2.2, the optimized torsional spring stiffness should be $26.635\frac{N \cdot m}{rad}$. The spring stiffness the manufacturers could provide was $26.5\frac{N \cdot m}{rad}$ which is close enough to the optimized value.

A motion simulation and a finite element analysis were performed in previous work to verify that the designed four-bar mechanism has the ability to withstand the external force during normal walking [13]. The total weight of the prosthesis is 2.23kg which is fit for the amputee users weighing between 81.8∼90.9kg.

2.3.2 Prototype Fabrication and Bench Testing

The parts were fabricated and assembled according to the specifications of the designed active and passive components. The prototype of the transtibial prosthesis is shown in Fig. 2.3. The prosthesis has a height of 197mm and is only

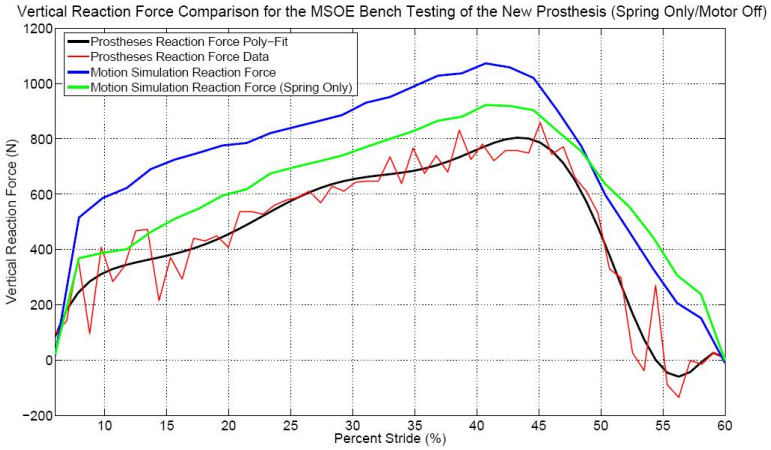

Figure 2.4: The Results of the Bench Testing of the Transtibial Prosthesis with the Active Components Turned Off

2.58% of the target amputee's weight. The designed range of motion is from 60° plantar flexion to 20° dorsiflexion, which exceeds that of an able-bodied person.

In order to obtain some preliminary testing data to verify the design concept of this prosthesis, bench testing was performed on a standard static tensile testing machine. The details of the testing protocol are described in [13]. During the testing, the ground reaction force (GRF) was measured using a vertical axis force transducer.

The testing results is shown in Fig. 2.4. The results show that, when the active components were turned off, with only the four-bar mechanism and the torsional spring, the prosthesis was capable of producing 80.1% of the desired GRF. It proves that when the motor is turned on with the control system designed, the prosthesis will be able to produce the full ankle moment profile that an able-bodied person can produce.

CHAPTER 3

Overall Control Algorithm

As previously mentioned in Chapter 2, the bench testing showed that the four-bar mechanism with a torsional spring is able to generate about 80% of the required moment. About 20% of the moment needs to be provided from the motor. In this chapter, the dynamics of the human gait is first analyzed in order to design the control algorithm for the motor. Then, a two level control algorithm, which includes a higher level finite state machine and lower level PID controllers, is proposed to manage the gait process. The structure of each level of the controllers are further presented individually.

3.1 Dynamics of Human Gait

Human gait is a cyclical process which a person performs thousands of times every day. For an able-bodied person, one gait cycle starts from the initial heel contact with the ground of one foot and ends at the next initial ground contact of the same foot. During one gait cycle, about 62% of the time the foot has contact with ground, the rest of the time the foot has no contact with the ground and thus in swing. One gait cycle can be divided into two phases depending on if the foot has contact with the ground. One phase is the Stance Phase and the other is the Swing Phase.

The dynamic characteristic of the stance phase is summarized in Tab. 3.1. During the stance phase, kinematically, the foot makes physical contact with the ground. Kinetically, the ankle has two major functions during this phase. The first function is that the impedance of the ankle increases during the early stance phase and decreases during the late half of the stance phase, which helps the body to maintain dynamic stability and move forward. This function can be realized by the four-bar linkage and the torsional spring. The second function is that the ankle can

Table 3.1: The Selected Active Components

Phase	Sub-Phase	Foot/Ankle Kinematics	Foot/Ankle Function
Stance	Loading Response	Plantar Flexion	Shock absorption and rocker initiation
	Mid and Terminal Stance	Dorsiflexion	Absorb energy and rocker for progression
	Pre-Swing	Plantar Flexion	Propulsion
Swing	Swing	Plantar Flexion until neutral	Return to neutral position

store energy and actively generates the extra required energy to help with the push off during the later stage. This second function will be realized by the motor and its control system.

The Stance Phase can be further divided into three sub-phases, namely Loading Response, Mid and Terminal Stance and Pre-Swing. Each sub-phase has its unique foot/ankle function, kinematic characteristics and different moment profile. The function of the Loading Response is shock absorption which is mainly realized by the mechanism and the torsional spring. Also during this sub-phase, the foot initiates its function as a rocker. Rocker in this case means the function of the foot as a rocker when the center of the mass of the human body progresses forward. The function of the Mid and Terminal Stance sub-phase is to store energy in the ankle as the calf progresses forward. Whether or not enough energy is stored inside the torsional spring determines if the prosthesis user has a normal push-off during the Pre-Swing sub-phase. Therefore, during this sub-phase, the motor should provide the extra required energy to help with the push-off.

During the Swing Phase, the foot does not make contact with the ground. The function of the foot/ankle during this phase is to restore the foot to the neutral position and get ready for the next heel strike. The characteristics of the swing phase is also listed in Tab. 3.1.

3.2 Proposed Control Algorithm

The purpose of the designed prosthesis is to help the amputees regain the dynamics of able-bodied gait. The proposed control algorithm therefore needs to satisfy the following requirements:

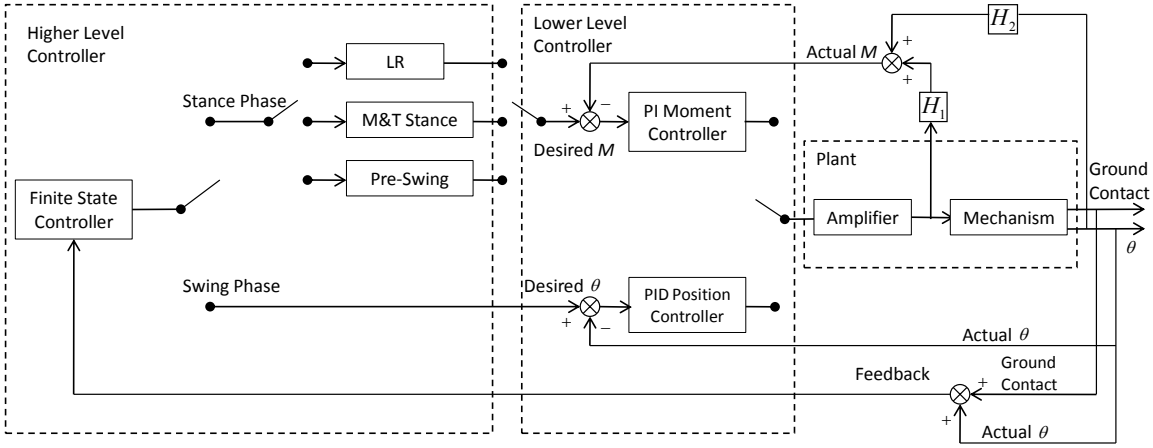

Figure 3.1: The Proposed Overall Control Algorithm

- Because human gait is a repetitive process, the controller should be able to change from the last state back to the first state and be cycled indefinitely.
- The controller should be able to identify which phase and sub-phase the prosthesis is in. Since each of the phase and sub-phase has its own kinematics feature, local sensing is favorable to perform gait detection and transition between phases.
- The controller should be able to work in different modes and switch between the modes swiftly. For example, when the prosthesis is in Stance Phase, the controller should control the moment generated in the prosthesis. When the prosthesis transitions to the Swing Phase, the controller should be able to switch to position control swiftly.

Based on these requirements, the proposed overall control algorithm should first be able to identify the status the prosthesis. When the prosthesis is in Stance Phase, the controller should generated the target moment profile (named "moment control mode"). When the prosthesis is in Swing phase, the controller should be capable of controlling the ankle position of the prosthesis (named "position control mode"). A two level control method, which includes a higher level finite state controller (FSC) and lower level PID controllers, is proposed. The block diagram of the proposed control algorithm is shown in Fig. 3.1. The details of the higher level FSC and lower level PID controls will be described in Sec. 3.3 and Sec. 3.4.

The higher level FSC should first be able to determine if the prosthesis is in Stance Phase or Swing Phase using ground contact feedback. If the prosthesis is in Stance Phase, the lower level controller will be working under the moment control mode. The FSC will go further to determine which sub-phase is the device in using the feedback of ground contact and the angle of the ankle. The target moment profile is different between each sub-phase. If the prosthesis is in Swing Phase, the lower level controller will be working under the PID position control mode.

The lower level PID controllers regulate the moment generated by the motor or the position of the motor. When the moment controller is working, the reference input is the target moment profile. The moment provided by the prosthesis is measured and fed back to the controller, which is subtracted by the reference input to decide how much moment the motor needs to generate. When the PID position controller is active, the reference input is the target neutral position of the prosthesis. The actual position of the prosthesis ankle is fed back to the controller. The controller regulates the motor to move to the target position.

3.3 Higher Level Controller Schematic

Before going into the details of the control algorithm, several conventions used in this project need to be clarified:

- The direction of plantar flexion is defined to be positive and that of dorsiflexion is negative;
- θ represents the angular position of the ankle;
- "H" represents the heel contact of the amputated leg;
- "H2" represents the heel contact of the sound leg;
- "T" represents the toe contact;
- "1" stands for having contact with the ground while "0" stands for having no contact with the ground.

- "Event" stands for a switch in the status of one of the contact sensors, which triggers the transition from one phase or sub-phase to another phase or sub-phase. For example, if the transition to the Swing Phase is triggered by the toe sensor changing from "1" to "0", that change of the status of the toe sensor is called an "Event".

- "Condition" stands for the current status of one or several of the contact sensors. It is used to determine if a transition is correctly triggered. For example, when the transition to the Swing Phase is triggered, if the status of heel is 0 and that of the natural heel is 1, the transition is rightly triggered.

- "Transition" is a controller status when the controller has exited one phase or sub-phase but has not entered the next phase or sub-phase, which means the controller is in an interim status. The event triggers the controller into the "Transition" status and the conditions determine if the controller should finish the "Transition" and enter the next phase or sub-phase.

Perry and Burnfield [11] described in detail how to recognize each phase and sub-phase of one gait cycle according to the kinematic characteristics. The sensing strategy used in this thesis is similar. The schematic of how the proposed FSC works is shown in Fig. 3.2. The transition between each phase and sub-phase is triggered by events and conditions. The specified event triggers the transition of one phase and move the controller to the transition status. Then the controller will go further to check whether or not the specified conditions are satisfied. If the conditions are also satisfied, the controller will complete the transition and change to the next phase; if the conditions are not satisfied, which means the event is mistakenly triggered, the controller will ignore the event and go back to the current phase.

The FSC is composed of two parts: stance phase control and swing phase control. The stance phase control contains three states and the swing phase control has one state. Beginning from the transition between the Stance Phase and the Swing Phase, the kinematic details are discussed as follows:

- The transition to the Swing Phase begins with the event of the toe leaving the ground (T = 1→0). At the same time, if H is 0 and H2 is 1, the transition will

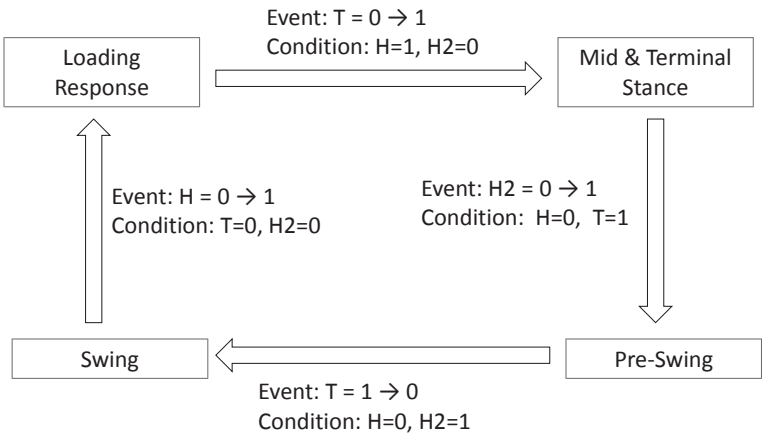

Figure 3.2: The Proposed Finite State Machine Working Schematic

be completed and switch to the swing phase control from the stance phase control.

- The transition to the Stance Phase control, specifically the Loading Response state, begins when the heel touches the ground (H = 0→1). Meanwhile, if T is 0 and H2 is 0, the transition will be completed and switch to the Loading Response state of the stance phase control.

- The transition to the Mid and Terminal Stance state begins when the toe touches the ground (T = 0→1). Meanwhile, if H is 1 and H2 is 0, the transition will be completed and switch to the Mid and Terminal Stance state.

- The transition to the Pre-Swing state begins when the natural leg touches the ground (H2 = 0→1). At the same time, if H is 0 and T is 1, the transition will be completed and switch to the Pre-Swing state.

- The transition to the Swing Phase will happen again if the previously specified event happens and conditions are satisfied.

The main focus of this work is to realize normal walking first, therefore, the other patterns like running or walking backwards are not considered. If the testing subject does something unknown, i.e., walking in some pattern the controller does not recognize, the control system will be automatically shut down and the prosthesis will work completely as a passive device.

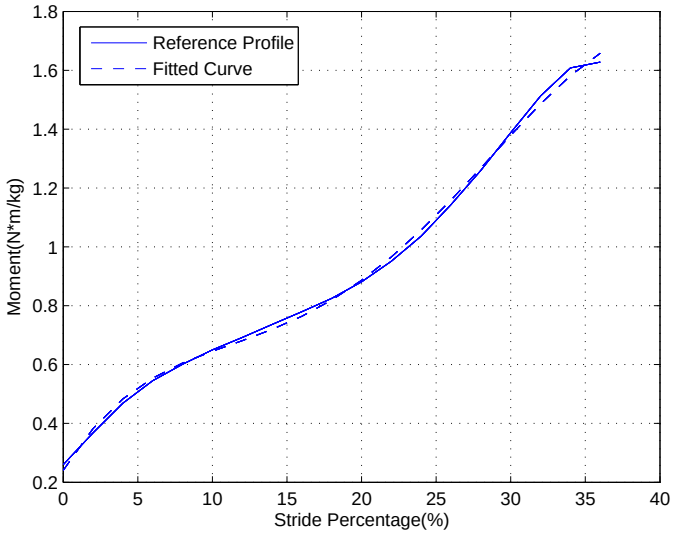

Figure 3.3: The Fitted Curve Compared to the Reference Moment

3.4 Lower Level PID Controllers

Once the higher level FSC has identified the phase and sub-phase status of the prosthesis, the corresponding lower level PID controller starts to perform. Classical PI control is used to regulate the moment during the stance phase control and PID control is used to regulate the position during the swing phase control. PID control has the advantage of being stable, robust and easy to implement. A more sophisticated lower level control algorithm may be used for future improvement, however, simplicity was taken as the first goal in this project.

3.4.1 PI Moment Controller

The design of the PI moment controller involves two procedures. The first one is the curve fitting of the nonlinear reference moment profile. The second is using dynamics to calculate the amount of moment the motors need to generate in real-time.

Reference Moment Curve Fitting

As described in Section 3.1, the Mid and Terminal Stance sub-phase is critical because the motor needs to actively generate moment. To regulate how

much moment needs to be generated from the motor, the reference moment profile must be known. The human gait data from Winter [7] is widely recognized and used in academia; therefore, it is selected to be the benchmark of the target ankle moment profile. However, this ankle moment is a nonlinear profile with regard to time and the data from [7] is given as sampled points in discrete time steps. The values between each two sampled points are unknown which will be difficult for the PID controller to follow. Therefore, curve fitting is used to approximate the nonlinear moment profile with a polynomial position, thus the target profile becomes continuous which will make the control system work much faster in real-time.

The built-in function "polyfit" in MATLAB was used to fit this profile to a fifth order polynomial. The reference profile and the fitted curve are shown in Fig. 3.3. The mean squared error is 2.6114e-4N*m/kg and the Pearson correlation coefficient is 0.999, which means the fitted curve is a good replacement of the reference moment profile.

Calculate the Moment from the Motor

The motor, which does not directly act on the ankle joint A as shown in Fig. 3.4[1], acts on joint C instead and therefore indirectly acts on joint A through the four bar mechanism. Therefore, even though the moment at the ankle joint A is obtained, the equivalent effective moment has to be converted to joint C using four bar mechanism kinematics. According to [25], the total moment at the ankle joint can be expressed as:

$$M_\theta = M_\phi \frac{\dot{\phi}}{\dot{\theta}} = (M_0 + M_{motor} + k\phi)\frac{\dot{\phi}}{\dot{\theta}} \tag{3.1}$$

where M_θ is the total moment at the ankle joint, M_ϕ is the moment measured at joint C, θ and ϕ are defined in Fig. 3.4, M_0 is the optimized preload in the torsional spring at the position $\theta = 0$ as shown in Eqn. 2.2, M_{motor} is the moment that needs to be generated from the motor, and k is the optimized torsional spring stiffness.

[1]Fig. 3.4 is a replication of Fig. 2.2 for convenience

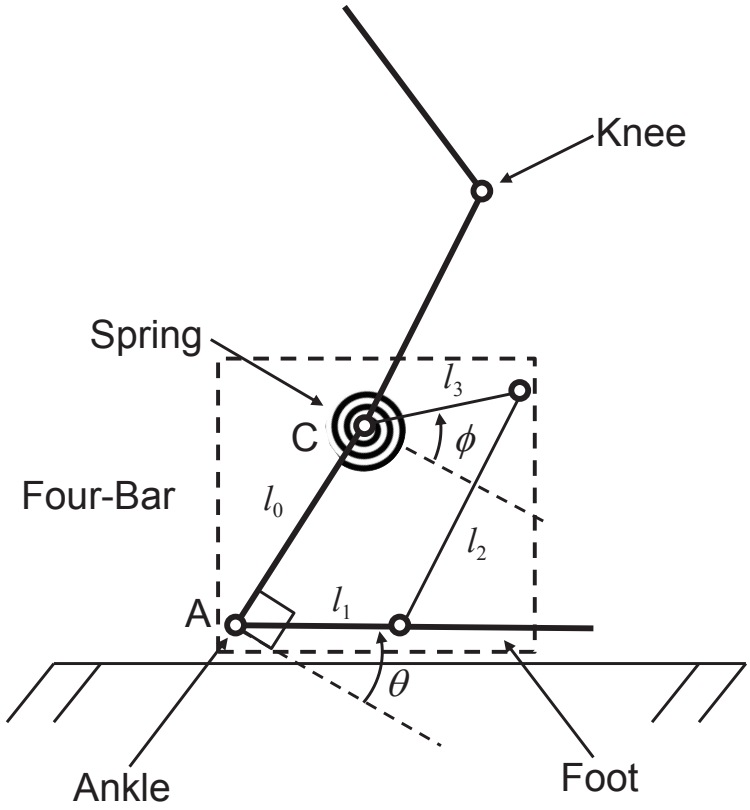

Figure 3.4: The Sketch of the Mechanism Design Concept

Rearranging Eqn. 3.1, the term M_{motor} can be made explicit:

$$M_{motor} = M_\theta \frac{\dot{\theta}}{\dot{\phi}} - k\phi - M_0 \tag{3.2}$$

In Eqn. 3.2, M_θ, k and M_0 are all predefined or optimized. ϕ will be measured by the sensor. Therefore, the only unknown is the fraction of the angular velocities $\frac{\dot{\theta}}{\dot{\phi}}$. Because θ and ϕ are two angles in a four-bar mechanism, they are not independent with each other and have certain relationships. ϕ can be measured by the sensor, the term $\frac{\dot{\theta}}{\dot{\phi}}$ can be obtained with the four-bar mechanism kinematics derived in Norton [26]. The details of this derivation is shown in Appendix. A. Therefore, the moment needs to be generated from the motor can be calculated in real-time.

3.4.2 PID Position Controller

The function of the PID position controller is to move the prosthesis ankle back to the neutral position during the Swing Phase to get ready for the next heel

strike. Unlike the PI moment controller, the reference input of this PID controller is a constant position, therefore, its structure is simpler. The feedback signal is angle ϕ at joint C as shown in Fig. 3.4. The ankle angle θ can be obtained from ϕ since they have a kinematic relationship which was derived in the section above. The block diagram of this PID position controller can be seen in Fig. 3.1.

The time duration of the swing phase is only about 0.4 sec, which means the controller has to respond quickly. Therefore, the PID parameters need to be adjusted so that the rise time to a step input is small.

3.5 Conclusion

In this chapter, a two-level control algorithm is proposed which includes a higher level FSC and lower level PID controllers. The FSC can identify which phase and sub-phase the prosthesis is in and the lower level PID controllers are able to either generate the required target moment profile or move the prosthesis to the target position. The expression of the moment needed to be generated from the motor is derived so that the PID controller is able to work in real-time.

CHAPTER 4

Control System Realization

The designed control algorithm needs to be realized both in hardware and software. The hardware system consists of four parts: a higher level finite state controller, lower level PID controllers, sensors and power supplies. The whole hardware system is laid out onto a backpack which is convenient for the amputee to carry during the testing. The hardware realization of the designed controller is discussed in the front part of this chapter. The software programming of the control algorithm and the communication between the different hardware component are described in the second part.

4.1 Hardware Configuration

Four criteria are important when selecting the hardware. The first is that it must be able to provide the required function as described in the control algorithm design. The second is that, because the whole system will be carried by the amputee while walking, the device must be lightweight and small so that the system is portable. The third is that the controllers should be easy to program and use.

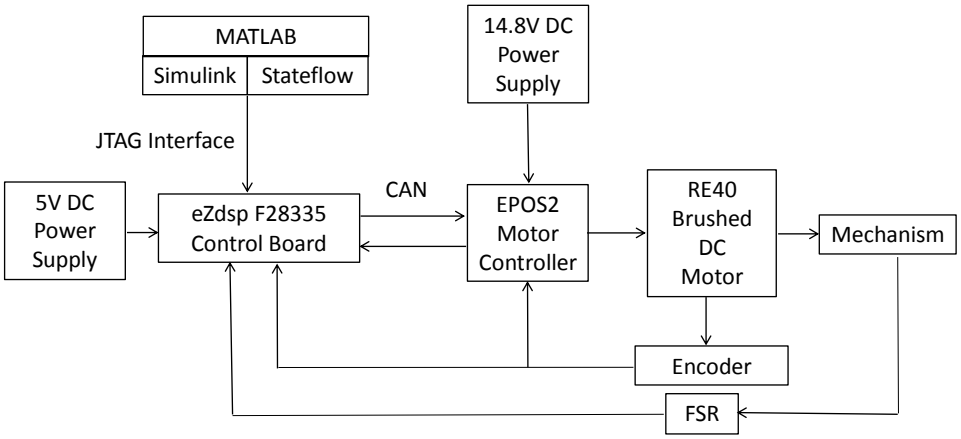

Figure 4.1: The Hardware System Configuration

The fourth is that the cost of components have to be within a acceptable range for budget consideration. Based on these criteria, the devices are selected and organized as shown in Fig. 4.1. Each of the components will be explained in the following sections.

4.1.1 Higher and Lower Level Controller Hardware

The hardware of the higher level FSC is realized by using a DSP control board. An eZdsp F28335 control board from Spectrum Digital Inc. was selected to be the processing unit for the control system. The microprocessor mounted on this control board is a TI TMS320F28335 DSP. The clock frequency of this microprocessor is 150MHz which means it is very fast in signal processing. It can interface with MATLAB Simulink therefore it is easy to build and revise the control program. The size of this control board is 135×75mm and its weight is negligible. The most important advantage of this DSP is that it has a complete set of peripherals which includes an analog to digital converter (ADC), general purpose input/output (GPIO), controller area network (CAN) bus, serial communication interface (SCI) and several other peripherals [27]. These functions will greatly facilitate the implementation of the control system.

A Maxon EPOS2 50/5 positioning motor controller was selected to realize the lower level PID controllers' function. The best feature of this controller is that it is able to work under multiple control modes. It can work under the current control mode, in which the moment generated by the motor will be regulated by regulating the armature current. This will realize the proposed prosthesis function during the Stance Phase. It can also work under the position control mode, under which the angular position of the motor is regulated. This will realize the prosthesis function during the Swing Phase. The switching between the two modes can be realized by easily changing the registers in the motor controller.

Another advantage of this controller is that it has a CAN port which can quickly communicate with the controlling DSP. CAN communication is a message based protocol widely used in the automation industry. It is a digital communication, has strong anti-jamming ability, which makes the control precise.

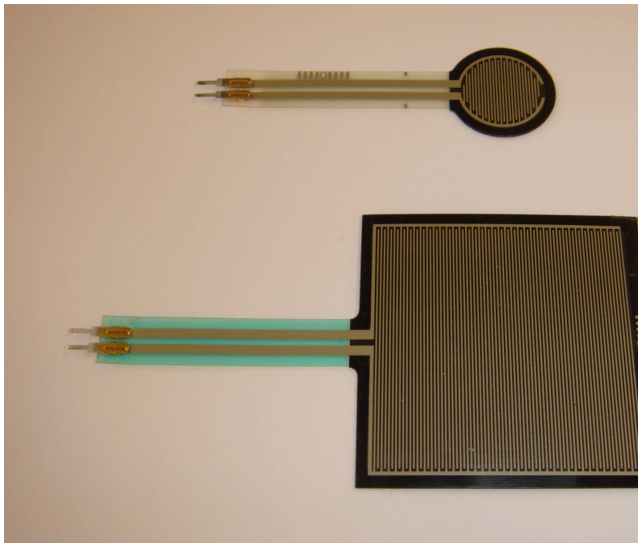

Figure 4.2: Force Sensing Resistors

Its bit rate can be up to 1Mbits/sec therefore the time delay is negligible. The DSP can conveniently switch the registers (and thus the working mode) of the EPOS2 50/5 controller by sending CAN messages. By specifying the eZDsp F28335 control board as the master machine, and the EPOS2 50/5 as the slave machine, the backbone of the control system is established.

4.1.2 Sensors

As mentioned in Chapter 3, sensors are necessary to provide the required foot contact information between the toe/heel and the ground. The angular position and velocity of the motor needs to be fed back in real-time. The angular displacement of the torsional spring and four-bar mechanism are also required. In addition, the current running through the motor armature needs to be fed back inside the lower level control loop to make it possible to realize current control.

A piezoelectric type of sensor called a force sensing resistor (FSR) (shown in Fig. 4.2), was selected to provide ground contact feedback to the DSP processor. The working principle of this type of sensor is that its resistance decreases significantly when external force is exerted on its surface. Its standoff resistance is greater than 1MΩ, while the resistance drops to smaller than 1kΩ if a force more than 10N is exerted. It cannot be used for precise force measurement since the

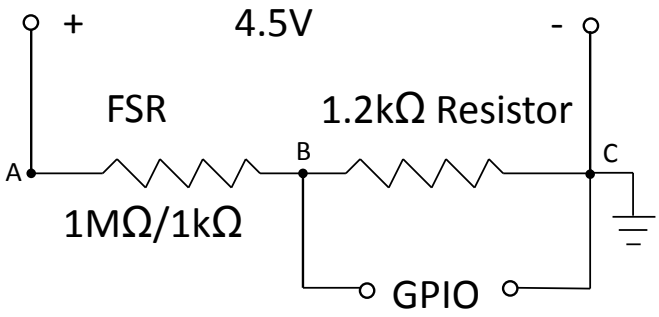

Figure 4.3: Accompanying Electric Circuits for the FSR Sensors

force-resistance curve is nonlinear and the magnitude of the measurement is dependent on the position the force exerted on the sensor.

An accompanying electrical circuit had to be built to make use of the FSR. The circuit is shown in Fig. 4.3, where the FSR is connected in series with a 1.2kΩ resistor and the GPIO measures the voltage at point B. When there is no force or negligible force on the FSR, its resistance is around 1MΩ, therefore the FSR will have a large voltage drop and the voltage across BC (i.e., V_{BC}) will be close to zero; the GPIO will show 0. If a force more than 10N is exerted on the FSR, its resistance is less than 1kΩ. Therefore, the resistor will have a significant voltage drop which will be more than 2 Volts; V_{BC} will show 1. Using this simple circuit, the contact between the heel/toe of the prosthesis and the ground can be detected.

The angular position and velocity of the motor shaft can be measured by an encoder. The encoder used in this work is three-channel incremental encoder which has 500 counts per revolution. It is directly mounted on the shaft of the brushed DC motor, therefore the angular position and the velocity of the motor can be measured. As previously described in Chap. 2, the motor shaft is connected to the torsional spring and Joint C of the four-bar mechanism through a 50:1 gearbox. Therefore, using the angular position measured by the encoder can indirectly measure the angular position of the torsional spring and the four-bar mechanism.

There is a built-in current sensor inside the EPOS2 50/5 motor controller, which is capable of measuring the current running through the motor armature. As described in Chap. 3, the higher level FSC also required the feedback of the current to calculate control input. The current feedback signal can be realized by using

Table 4.1: Controller Phase Corresponding to Sensor States

	Toe(T)	Heel(H)	Natural Heel(H2)
Swing	0	0	1
Loading Response	0	1	0
Mid and Terminal Stance	1	1	0
Pre-Swing	1	0	1

CAN communication between the DSP and the EPOS2 controller. The moment generated by the motor is proportional to the current running through the motor armature, therefore, the moment generated by the motor can be calculated.

Using the FSR sensors, the encoder and the built-in current sensor, all the required feedback is provided. The advantages of using these sensors are that they all are light, easy to use and do not consume much energy.

4.2 Software Programming

The control system is also to be realized in software. Of the two levels of the controller, the majority of the programming work is done on the DSP controller, since it functions as the master in the control system. The lower level EPOS2 50/5 works as a slave. It is controlled by the master by changing the values of its registers. Therefore, the EPOS2 controller does not require programming.

The programming of the DSP can be divided into two parts. The first part is the realization of the higher level control algorithm described in Chap. 3. The second is the programming of the lower level controller in which DSP sends commands to the EPOS2 50/5 controller using CAN communication. Both parts are realized by using MATLAB Simulink where the Embedded Coder toolbox in Simulink can automatically generate equivalent C code which can be downloaded to the DSP. It is more convenient to program and revise in this way than directly programming in C.

4.2.1 Higher Level Control Algorithm Programming

As mentioned previously in Chap. 3, what phase the controller is in depends on the states of the contact sensors. The details of this information are listed in

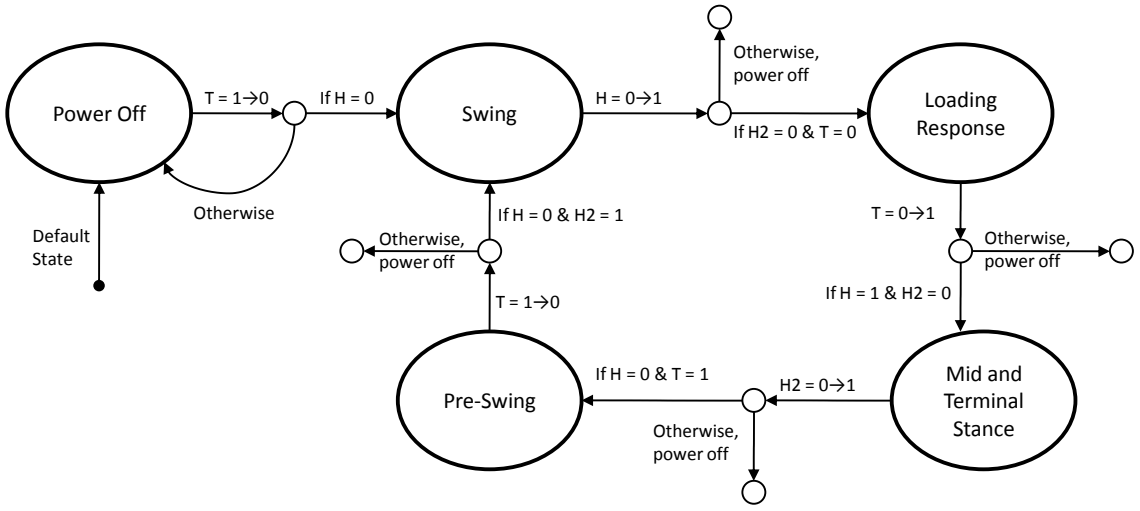

Figure 4.4: Complete Higher Level Control Flow Graph Considering Different Situations

Tab. 4.1. The designed higher level FSC scheme as shown in Fig. 3.2 is incomplete because it does not include all the abnormal situations. For example, when the controller is in the Loading Response sub-phase, if the amputee stops walking, the heel will change from 0 to 1 instead of the supposed toe changing from 0 to 1 in normal gait. This will cause malfunction in the FSC since the controller does not recognize this pattern. Therefore, the FSC needs to be robust and consider abnormal situations during normal walking. The complete FSC scheme is shown in Fig. 4.4. In this updated control scheme, if something abnormal happens during the subject testing, the controller will automatically shut down and the prosthesis will work completely as a passive mechanism albeit in a plantar flexed position.

The proposed higher level FSC control algorithm was programmed in Simulink using the Stateflow toolbox. The complete control flow graph is shown in Fig. B.2 in Appendix. B. The Stateflow toolbox is a design environment in which logic can be programmed in the way of drawing state charts or flow diagrams, thus making the programming of complex logic natural, readable and understandable. The similarity can be noticed between the designed control algorithm block diagram in Fig. 4.4 and the Stateflow control program in Fig. B.2, which partially explains why Simulink was chosen.

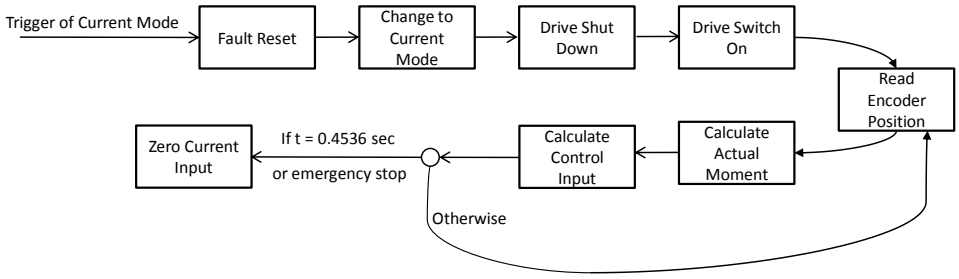

Figure 4.5: PI Moment Control Block Diagram

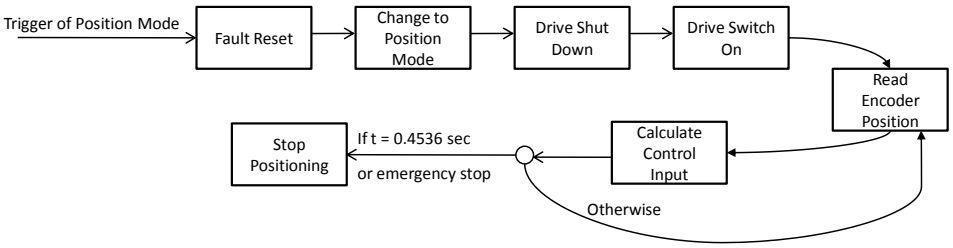

Figure 4.6: PID Position Control Block Diagram

4.2.2 Lower Level Control Programming

The lower level control program is also built using the Stateflow toolbox. As mentioned in Chap. 3, the PI moment controller regulates the moment generated by the motor during the Stance Phase. During Swing Phase, the PID position controller regulates the position of the motor shaft. The complete control block diagrams of both the PI moment controller and the PID position controller are

Figure 4.7: The Backpack with All the Hardware Components

shown in Fig. 4.5 and Fig. 4.6 respectively. The control program built in the Stateflow toolbox are shown in Fig. B.3, Fig. B.4 and Fig. B.5 in Appendix A. Again the similarities can be seen between the block diagrams and the computer programs.

4.3 Portable Testing Platform

In order to perform the amputee subjects testing untethered in the gait lab, the hardware devices were made portable by mounting them on a plastic board which was mounted on a backpack frame as shown in Fig. 4.7.

Power supplies are added to the backpack for each electrical component. The eZdsp F28335 control board is powered by a 5V lithium-ion battery, which has 6600mAh capacity. The power consumption of the control board is less than 0.15mW/MHz [27]. Even if the DSP board is running at full capacity, the battery can last for more than 1000 hours. The EPOS2 50/5 motor controller is powered by a 14.8V lithium-ion polymer battery pack which has a capacity of 5100mAh. This motor controller also provides power supply for the brushed DC motor, therefore, the power consumption varies with the power consumption of the motor. A rough estimation of the power consumption of the motor controller and the motor can be 2000mAh. This battery still can last for more than 2 hours which satisfy the testing need. The FSR sensor circuits are powered by three 1.5V standard AAA batteries connected in series.

The size of the control system is not a critical aspect since this is the first iteration of the prototype. The control system was built on a spacious plastic board for the convenience of adding and removing components. The system will be made more compact in the future.

4.4 Conclusion

In this chapter, the control system was built. The hardware of the control system includes a DSP control board, a EPOS2 50/5 motor controller, FSR sensors and their accompanying circuits, and power supplies. The software of the control system was realized by programming in MATLAB Simulink and Stateflow toolbox.

The communication between the master DSP and the slave EPOS2 controller is realized by using CAN. The control program can be automatically converted to C code and downloaded to the DSP board. The whole control system was implemented on a backpack which will be carried by the amputee subject during the testing.

CHAPTER 5

Dynamic Modeling and Simulation

Modeling and simulation are well recognized both in academia and industry. It can help reduce the cost and increase the quality of the products. For this project, building a dynamic model and performing the simulation can help find potential problems. In addition, the PID parameters of the lower level controllers need to be determined. The simulation can provide a benchmark for the final PID parameters used in the real control system. In this chapter, several assumptions are first made to simplify the process and make the modeling easier. Then, the dynamic model are built and simulated using MATLAB Simulink. Third, the PID parameters of the lower level controllers are tuned to make the controller able to regulate the motor to generate the reference moment or move to the target position.

5.1 Assumptions

A necessary first step in any modeling is to make reasonable assumptions. These assumptions will help neglect the trivial details which are usually difficult to model and focus on the important parts. In this project, the following assumptions were made:

1. By definition of the FSR, during Mid and Terminal Stance sub-phase in Stance Phase, the motor is under PI moment control. During Swing Phase, the motor is under PID position control. These are two separate controllers. Therefore, in the dynamic simulation, the lower level controls of the two phases are independent and will be separately modeled and simulated.

2. This project uses the gait data in Winter [7] as the benchmark, where the time span of one entire gait cycle is 1.134 sec. The same gait cycle period value is used in this thesis. The Mid and Terminal Stance sub-phase spans

38% of one gait cycle. Therefore, it is assumed that the time span during which the PI moment controller is working is $1.134 \times 38\% = 0.4309sec$. The Swing Phase spans from 62% to 100%, which is also 38% percent of one gait cycle. Therefore, the time span during which the PID position controller is working is the same 0.4536 sec.

3. The four-bar mechanism is the dynamic part of the prosthesis. The other components such as the gearbox and the foot plate only have an inertial effect when the prosthesis is working. Therefore, only the components of the four-bar mechanism are built in the simulation. The mass and moment of inertia of the other components are added to the corresponding four bar linkage but their geometric shapes are not physically modeled.

4. The mass of the four-bar mechanism, the foot plate, the motor and the gearbox are assigned according to [13]. The moment of inertia of these components are estimated according to the geometry and the calculated mass. The mass and moment of inertia of the motor, the gearbox are incorporated to Link 0. Therefore, the center of mass of Link 0 is outside of the body of Link 0 when performing the analysis.

5. There are damping and frictional effects in both the torsional spring and the four-bar mechanism. However, the value of the damping and friction coefficients are hard to determine and they are varying as the prosthesis progresses. Therefore, these effects are not modeled in this dynamic simulation. The PID gains of the lower level controllers are determined assuming the damping and friction coefficients are zero. They will be adjusted online when performing experiments.

6. Similar as the damping and frictional effects, there is energy loss in the brushed DC motor and the gearbox. The rated efficiency of the gearbox is 82% [28]. The efficiency of the motor is hard to determine since in this project, the motor is running at low speed. According to [3], the motor efficiency quickly drops below 50% when it is running below 2000 rpm or

above 0.2 Nm. In this dynamic simulation, the energy efficiency is initially assumed to be 100% for the convenience of PID gain tuning. The PID gains will be further adjusted when performing experiments.

7. In the previous work, the optimization of the torsional spring and the four bar mechanism was performed based on the assumption that the prosthesis will perform the same kinematics as an able-bodied person while being worn by an amputee, which means the ankle angle will be the same function of time. Therefore the same assumption is made in the control system design.

8. When performing the dynamic simulation, the control signals coming out of the PID controller are assumed to be ideal sources. In reality, the forces will come from the brushed DC motor. There will be time lag in the response of the motor which is not modeled.

5.2 Four Bar Mechanism Modeling

There are two ways to model the dynamic process in this project. The first is to utilize first principles to derive the governing equation and build the model in the form of a series of differential equations. Because the major mechanical components of the prosthesis are a four-bar mechanism, the differential equations will be highly nonlinear and nonhomogeneous. Using numerical methods, e.g., the Runge-Kutta method, one should be able to compute the numerical solution of these equations. Utilizing the power of current computational technology, the second way to build the model is to use computer software to build the physical model of the prosthesis and let the software derive the governing equations and solve them numerically in the background. These two methods are essentially the same, but the latter one is much more convenient to use. In addition, one another advantage of using the second method is that the mechanical model can be visually viewed. Therefore, using software to model and simulate the dynamic process is utilized in this project.

SimMechanics toolbox in MATLAB Simulink was particularly useful in this dynamic simulation to build the plant model. SimMechanics is a multi-body simulation environment for 3D modeling, such as robots, vehicles and aircrafts. The

models are built in a intuitive way by dragging blocks to represent bodies, joints, constraints and forces. An additional advantage of using SimMechanics is that electrical control models such as PID controllers and reference signals can be linked with the SimMechanics model in a seamless way in one single simulation model [29].

5.2.1 Stance Phase Modeling

As mentioned in the assumptions, the Stance Phase and the Swing Phase will be separately simulated. The kinematics and kinetic functions of these two phases are different as shown in Tab. 3.1, so the SimMechanics model will be adjusted accordingly. Another assumption made is that the prosthesis during Mid and Terminal Stance sub-phase will have the same kinematics as an able-bodied person. During Mid and Terminal Stance sub-phases, both the heel and toe of the prosthesis should have contact with the ground. The entire footplate should have no movement at all while the leg progresses forward. Therefore, Link 1 as shown in Fig. 3.4, which together the foot plate, will be modeled as the ground link. An able-bodied person's ankle angular position profile as a function of time is assumed to be provided to the ankle joint of the prosthesis. The moment generated at Joint C (Fig. 3.4) is going to be the feedback. The moment at Joint C will be controlled to generate the equivalent reference ankle moment at the ankle joint.

The SimMechanics model of the prosthesis in Stance Phase is shown in Fig. 5.1. There are three parts in the model: The torsional spring, angular position input and the four-bar mechanism. The four-bar mechanism was built using SimMechanics toolbox. The torsional spring and the angular position input were built using standard Simulink blocks. The standard Simulink blocks interface with the SimMechanics blocks seamlessly through Body/Joint Actuator or Sensor blocks. One another advantage of using Simulink is that the mechanical model can be visually viewed. The illustration of the mechanism built in Fig. 5.1 is shown in Fig. 5.2, which shows the initial position of the mechanism when the Mid and Terminal Stance sub-phase starts.

Two things should be noted in this model. The first is that Link 1 is not shown in Fig. 5.2 because it functions as the ground link with the foot plate. The

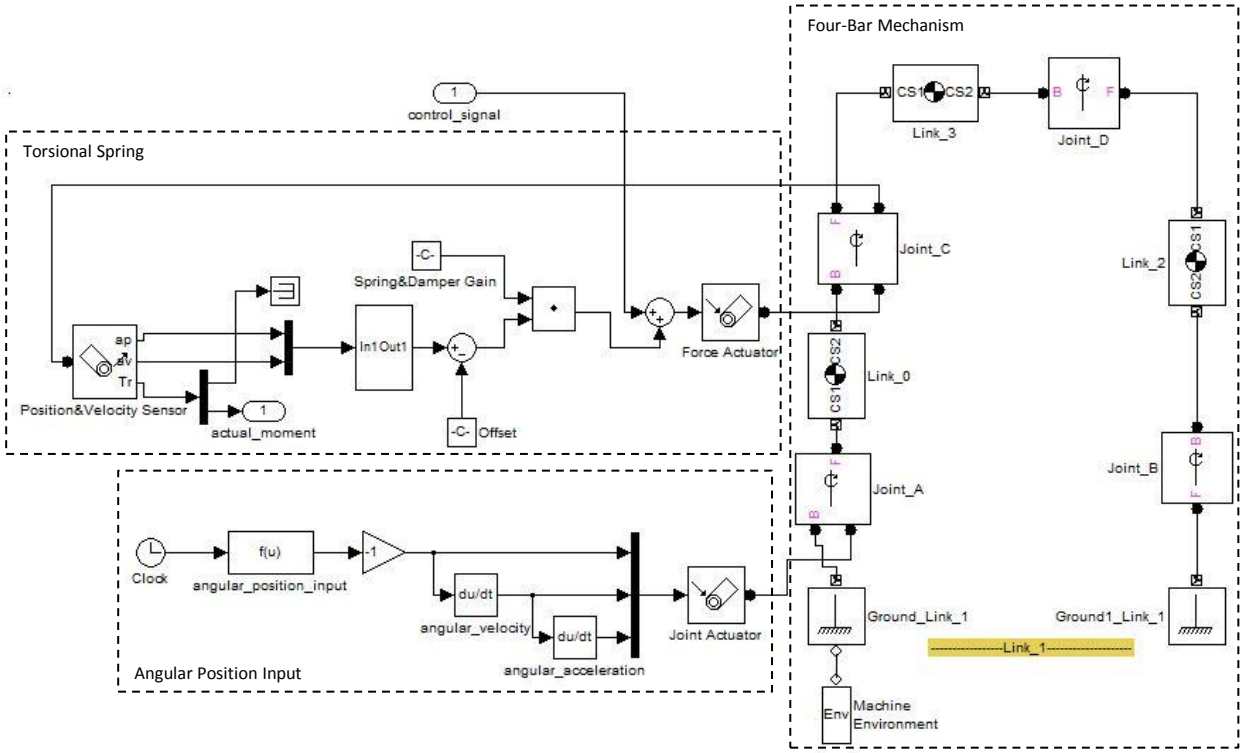

Figure 5.1: SimMechanics Model of the Prosthesis during Stance Phase

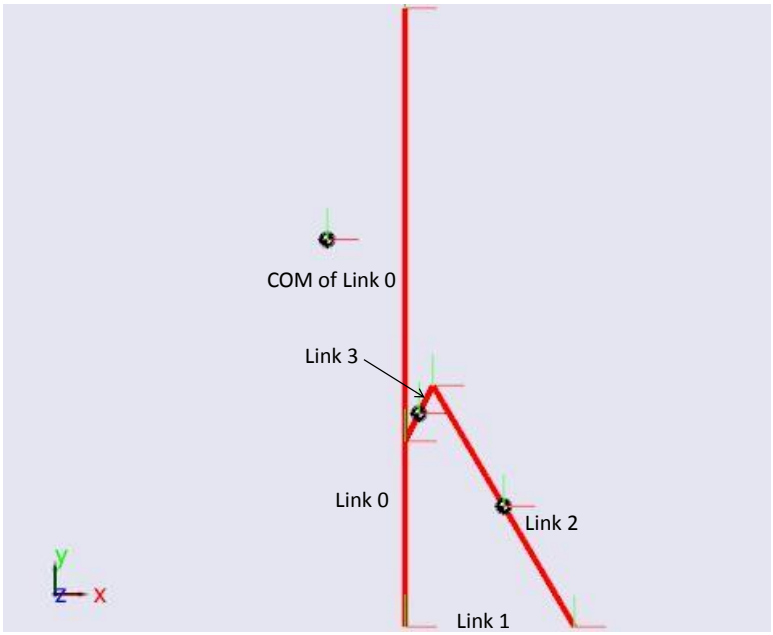

Figure 5.2: The Stance Phase Prosthesis Model Built in Fig. 5.1

second is that the center of mass of Link 0 is out of the body, because the inertia properties of the gearbox and the motor are incorporated into link 0 as mentioned in the assumptions.

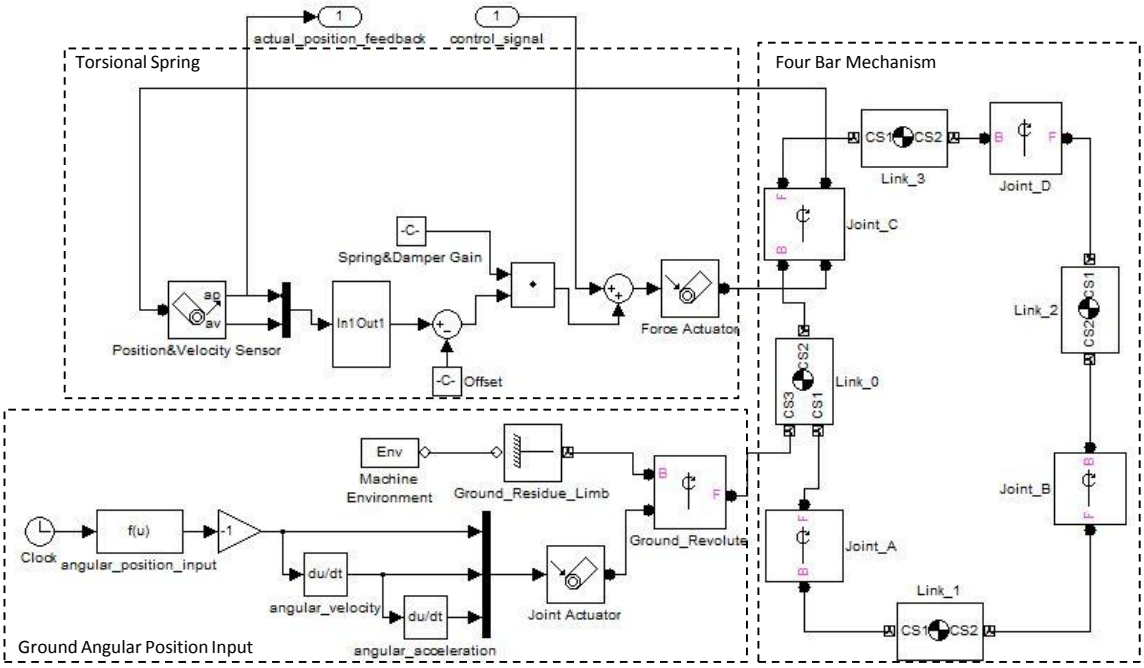

Figure 5.3: SimMechanics Model of the Prosthesis during Swing Phase

5.2.2 Swing Phase Modeling

The mechanism model during the Swing Phase is different in that Link 1 is not fixed to the ground anymore and it swings with the whole mechanism. The ankle needs to go back to the initial position of one gait cycle to get ready for the next heel strike. Therefore the angular position of Joint C functions as the feedback during the Swing Phase and it is controlled to generate the required position at the ankle joint, Joint A. The top of Link 0 is considered as the ground because it is fixed to the amputee's residual limb. A predefined angular position profile drives the ground revolute joint so that the entire prosthesis model swings as an able-bodied person during the Swing Phase.

The SimMechanics model of the prosthesis during Swing Phase is shown in Fig. 5.3. There are three parts in this model, which are the same as that of the Stance Phase model. The differences lie in that, first, the predefined angular position input is connected to the ground revolute joint instead of Joint A. Second, Link 1 is explicit in Swing Phase since it is not grounded anymore. The mechanical model built in Fig. 5.3 is illustrated in Fig. 5.4, which shows the mechanism in its initial position when the Swing Phase begins.

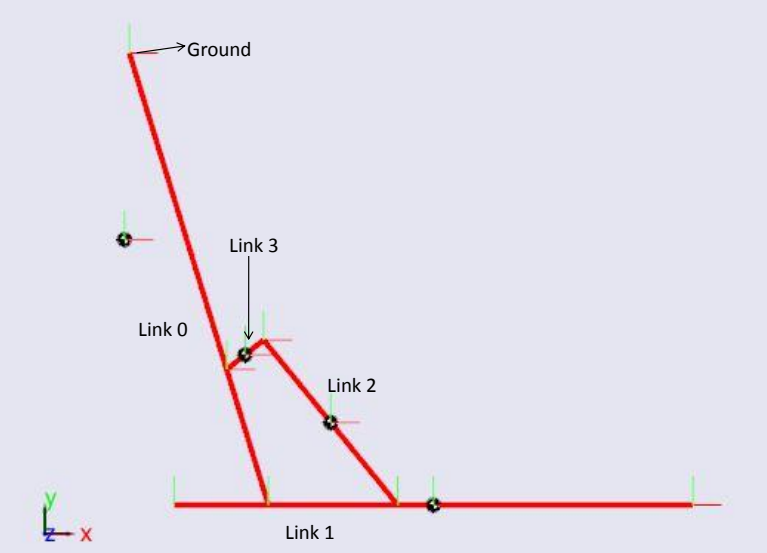

Figure 5.4: The Swing Phase Prosthesis Model Built in Fig. 5.3

Table 5.1: The Adjusted PID Gains of the Lower Level Controllers

	Stance Phase Control	Swing Phase Control
P-Gain	575	123
I-Gain	153	1400
D-Gain	N/A	60

5.3 Dynamic Simulation and PID Tuning

After the modeling of the four bar mechanism was completed for both the Stance and Swing Phase, control systems need to be added. A PI moment controller and the reference moment profile need to be incorporated into the Stance Phase simulation. A PID position controller and the reference position reference need to be incorporated into the Swing Phase simulation. The simulation can thus be performed and the PID gains for both controllers will be determined. A traditional way to determine the PID gains is to derive the linearized model from the plant and then determine the PID gains from the derived model. However, the four-bar mechanism cannot be linearized at one specific operating point as the nonlinear plant shifts significantly during the process. Therefore, the PID gains are adjusted using dynamic simulation.

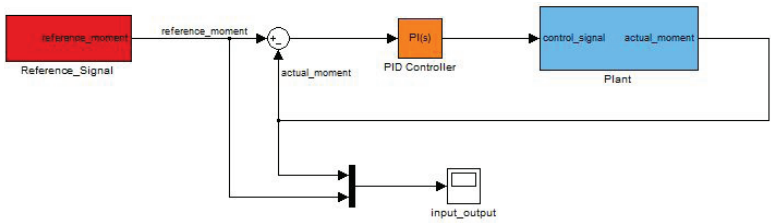

Figure 5.5: The Entire Stance Phase Simulation Model

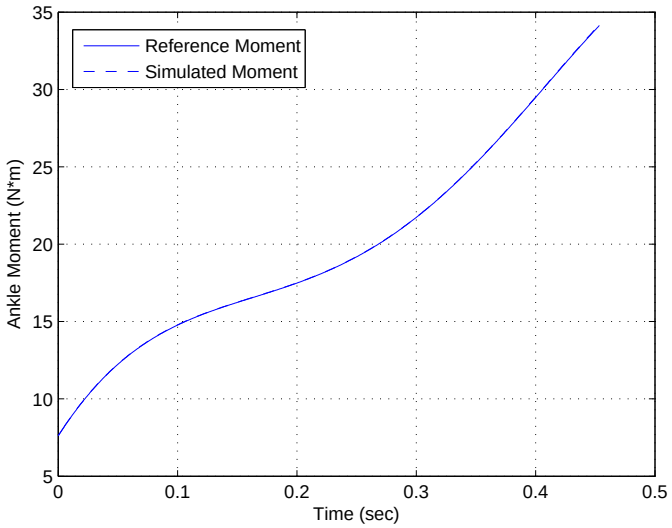

Figure 5.6: The Simulation Result of the Ankle Moment during Stance Phase

5.3.1 Stance Phase Simulation

The curve-fitted reference moment, which was developed in Section. 3.4, is used as the reference moment in Stance Phase simulation. Simulink has a built-in PID control block which can let the user customize the parameters and help the user auto tune the PID gains. This block was utilized in this simulation. The entire Stance Phase simulation model is shown in Fig. 5.5. The four-bar mechanism plant model built in Fig. 5.1 is made a subsystem as the blue block. The simulation was tested repeatedly and the PI gains were adjusted using both the classic Ziegler-Nichols method and the auto tuning function that was built in Simulink. The adjusted PI gains for the moment controller is shown in Tab. 5.1. The simulation result, which is the simulated ankle moment compared with the reference moment profile, is shown in Fig. 5.6. It can be noticed that the reference and the simulation ankle moment are identical to each other, which means in theory, if

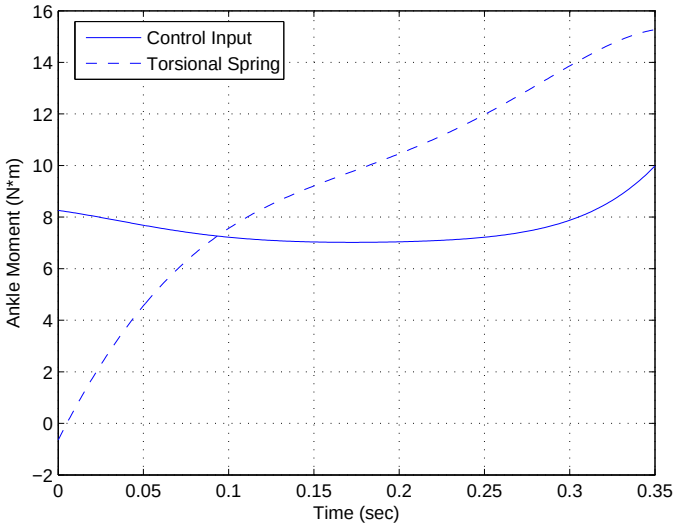

Figure 5.7: Decomposed Simulation Result of the Ankle Moment during Stance Phase

excluding the friction, damping effects and energy lost in the components, the device will perfectly perform as a human ankle during Stance Phase.

Fig. 5.7 shows the simulated ankle moment generated from the torsional spring and the control input separately. It can be seen that the moment contributed by the torsional spring is more than the contributed by the control input, which is consistent with the previous work [13]. The maximum moment provided by the motor is around 10N*m, which is within the capability of the motor.

5.3.2 Swing Phase Simulation

The reference profile of the Swing Phase is easier to model than Stance Phase in that it is a constant reference instead of being a nonlinear profile. Using the equations derived in Section 3.4, it can be calculated that the angular position value of 0.699 rad at Joint C will make the angular position at the ankle joint to be at the reference position. Therefore, this value will be the reference for the Swing Phase simulation.

A PID controller was utilized in the Swing Phase. The most important characteristic of the response is the rise time because the duration of the Swing Phase is only 0.4536 sec and the controller needs to respond fast when the Swing Phase begins. The overshoot and the steady state error are less critical as long as

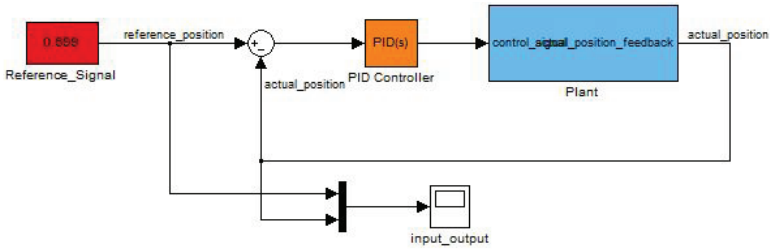

Figure 5.8: The Entire Swing Phase Simulation Model

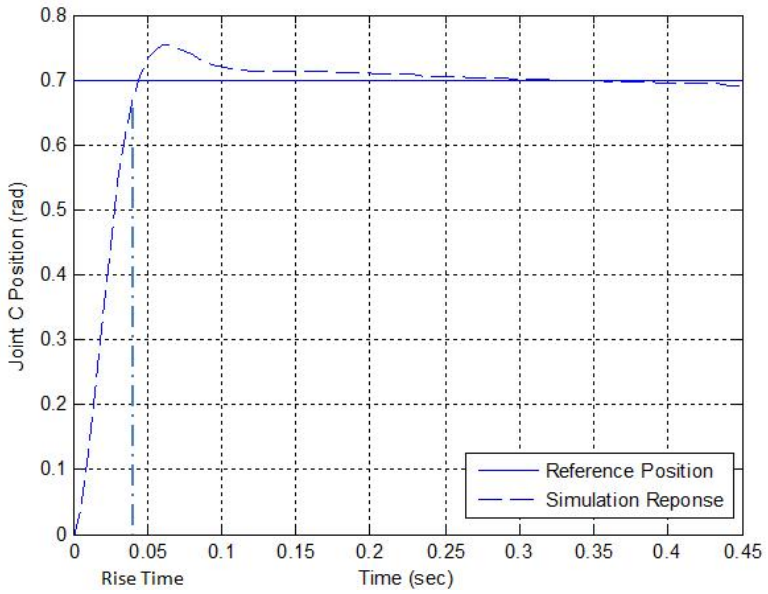

Figure 5.9: The Simulation Result of Joint C Position during Swing Phase

they are within an acceptable range. According to this requirement, employing the same method used in Stance Phase simulation, the PID gains were adjusted. The adjusted PID gains are listed in Tab. 5.1. The entire Swing Phase simulation model is shown in Fig. 5.8.

The simulation result with the adjusted PID gains is shown in Fig. 5.9. It can be seen that the most important rise time is only around 0.04 sec which satisfies the requirement. The overshoot is about 7% which is within the acceptable range and the steady state error is negligible. One thing that needs to bear in mind is that, because of the damping and friction effects inside the mechanism, the rise time will not get to as fast as 0.04 sec in the real experiment. But the adjusted PID gains in this simulation provides a good benchmark for the on-site PID gains tuning.

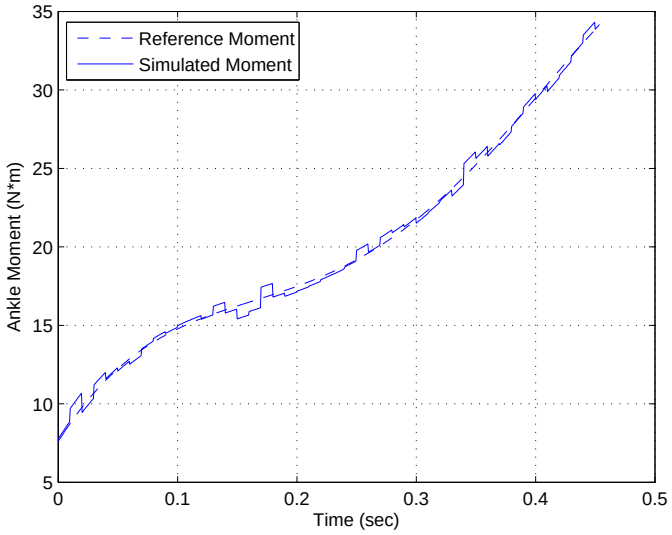

Figure 5.10: Stance Phase Simulation with White Noise

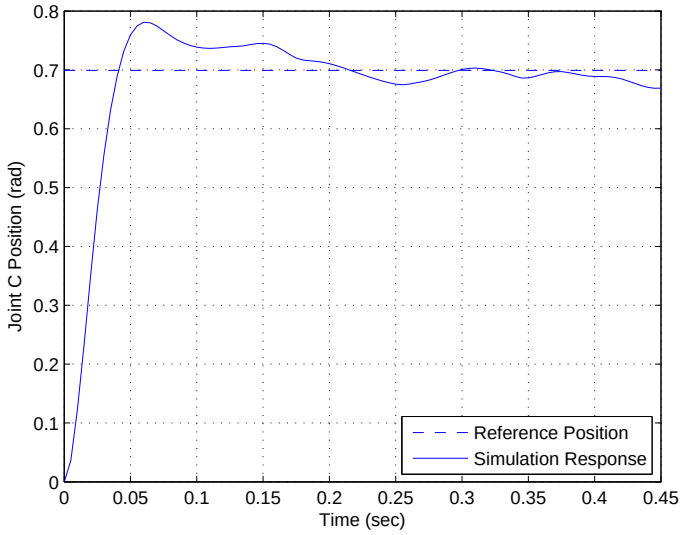

Figure 5.11: Swing Phase Simulation with White Noise

5.4 Robustness Testing of the Dynamic Model

During the amputee subject testing, the conditions under which the controller will be working is far from the ideal condition which is assumed in previous sections. In fact, there will be much noise on both the actuators and sensors. To test the robustness of the lower level controllers, white noise with a nominal power of 100W, which is assumed to be at the worst scenario, were added

to the dynamic model. For the Stance Phase simulation, the ankle moment output is plotted in Fig. 5.10. It can be seen that even though with the existence of the noise, the controller is still able to generate the reference ankle moment profile. For the Swing Phase simulation, Joint C angular position response is shown in Fig. 5.11. It can be seen that with the existence of the white noise, the PID controller could not get to the exact target position. However, the final position error is about 5.7% so it is still in an acceptable range. This simple testing shows that the designed PID controllers have the ability to resist the disturbances and noises to a certain level.

5.5 Conclusion

In this chapter, a computer based simulation of the dynamic process of the prosthesis in both Stance Phase and Swing Phase was performed. The dynamic model was built using MATLAB Simulink and SimMechanics. The simulation results shows that, under the simplified conditions, the PI moment controller and the PID position controller are able to regulate the prosthesis to perform the desired behavior. The robustness of the controllers are also tested. The results shows that, even with the existence of the disturbances and noises, the controller is still able to give the desired performance.

CHAPTER 6

Bench Testing and Amputee Subject Testing

To verify the ability of the motor to generate reference moment, bench testing was first performed. To evaluate the prosthesis and its control system in a real environment and obtain some experimental data, an amputee subject was tested performing level walking at self selected slow or moderate walking speed. Ramp ascent and descent walking was not tested since the first iteration control system is only designed for level walking. The testing methodology and procedures are first described. Then the results are illustrated and discussed from three different perspectives.

6.1 Moment Bench Testing

After the control system was realized, the performance of the mechanism and the control system was verified. However, directly testing the prosthesis on human subject is dangerous without any preliminary bench testing. Therefore, bench testing was performed to test the ability of the prosthesis to generate the reference moment in moment control mode.

During the bench testing, the control system is put into moment control mode. A reference input is given to the control system and the output of the actual generated moment at the ankle joint of the mechanism is measured. However, directly measuring the generated moment at Joint A (ankle joint) is difficult; the ground reaction force (GRF) is measured instead.

To make the reference moment data comparable to the measured GRF, the reference moment at Joint A is converted to the equivalent GRF in two ways. The first way is by deriving static equilibrium equations and solve these equations. The second way is by using CAD software to simulate the bench testing process. By inputting the reference moment into the simulation, the equivalent GRF is obtained.

Figure 6.1: Moment Bench Testing Configuration

6.1.1 Bench Testing Configuration

The bench testing was performed on an Instron machine. The setup of the testing is shown in Fig. 6.1. During the testing, the upper and lower end of the prosthesis are fixed to the two platens of the Instron machine. The platens do not move during the testing. A ramp moment reference signal up to 10Nm is input into the motor controller which generates a corresponding current to drive the motor. A load cell, mounted underneath the prosthesis on the lower platen measures the GRF. A bidirectional current sensor measures the current running through the motor armature. By measuring the current, the moment generated by the motor will be obtained.

6.1.2 Bench Testing Results and Interpretation

The results of the moment bench testing is shown in Fig. 6.2. The reference GRF results obtained from CAD simulation and static equations are consistent with each other. Hence they are considered as appropriate benchmark.

The solid line in Fig. 6.2 is the measured GRF from the load cell. It did not match the reference GRF from the static equations and simulation, and is on average 38% lower than the reference GRF. The main reason why the prosthesis is underpowered is due to the efficiency of the motor and gearbox. The rated efficiency

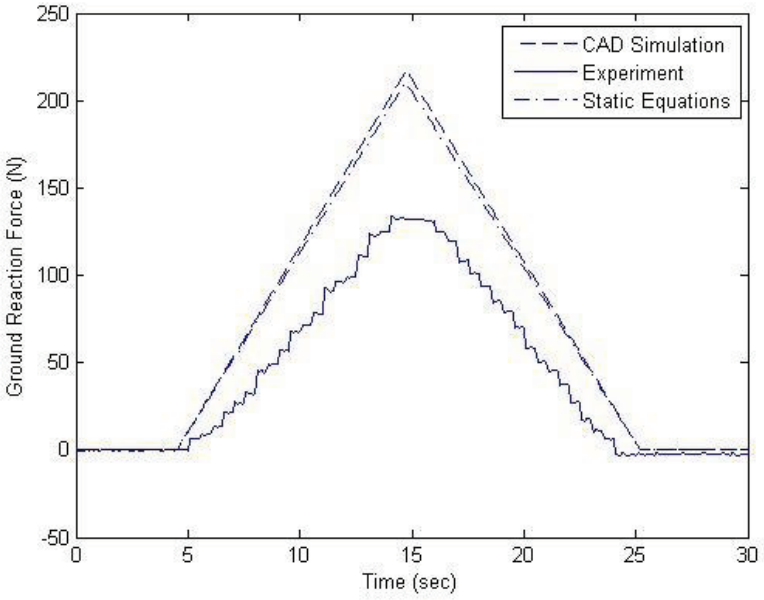

Figure 6.2: The Results of the Moment Bench Testing

of the gearbox is 85%, and the maximum efficiency of the motor is 92%. However, research [3] shows that when the brushed DC motor is working below 2,000 rpm and above 0.2 Nm, its efficiency quickly drops to below 50%, which is consistent with the bench test results.

The fundamental way to rectify this problem is by redesigning the components, such as using higher efficiency type of motor or using more sophisticated lower level control theory. However, since this is the first iteration prototype of the prosthesis and its purpose is to verify the design theory. No revision was taken for the first preliminary amputee subject testing. An easy method which can be used to temporarily rectify this problem is: To overpower the motor by an appropriate gain to compensate the efficiency problem. If the first preliminary amputee subject testing proves the capability of this powered prosthesis, a gain greater than one will be placed to overpower the motor for the following amputee subject testing until some fundamental revision is performed.

6.2 Amputee Subject Testing Method

The prosthesis was placed on the left leg of a healthy bilateral below-knee amputee. The amputee subject weighed 86.5kg and had been active since

amputation. The consent form was give to the amputee subject and the testing procedure was fully explained. Reflective markers were placed on the amputee subject to obtain kinematic testing data. A certified prosthetist was present during the testing. First, the subject walked using his own passive prosthesis. Then, the subject was allowed time to walk on the powered prosthesis to get used to it. The powered prosthesis testing began after the subject felt comfortable with it.

The testing was performed in the Medical College of Wisconsin Center for Motion Analysis. The subject was asked to walk across a 10 meter long path at his most comfortable speed. A Vicon system was utilized to capture the kinematics during the testing. Force plates on the ground along the walkway measured the GRF. The amputee subject was asked to ignore the existence of the force plates in order to reduce any changes in gait. The force and moment at each joint, the power consumption and other dynamic results were calculated using the standard inverse dynamics model and the measured kinematics and GRF. This process is automatically done by the Vicon system. A total of 15 trials were performed with the amputee subject wearing his original passive prosthesis. For most of the trials the subject did not fully step on the force plate, therefore, no satisfactory kinetic results were obtained for these trials. Only two trials the subject fully stepped on the foot plate, which means the complete dynamic results were obtained. The data from these two trial were used for data processing. For the powered prosthesis testing, 27 trials were performed and 3 trials yielded good dynamic results.

6.3 Amputee Subject Testing Results and Discussion

The testing results are to be interpreted from three perspectives. First, the results will be compared between each trial the amputee subject completed while wearing the powered prosthesis. The purpose of this comparison is to verify the consistency of the performance of the powered prosthesis. Second, the results will be compared between the powered prosthesis, the natural leg and the benchmark data from Winter [7]. The purpose of this comparison is to discuss if the performance of the powered prosthesis meets the design requirement and how its

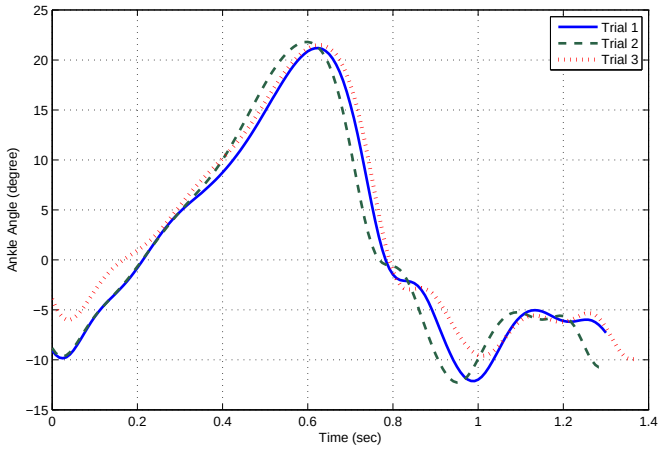

Figure 6.3: The Ankle Angle Comparison between the Three Trials of the Powered Prosthesis

performance is compared to the natural leg. Third, the results will be compared between the powered prosthesis and the passive prosthesis the amputee subject originally used. The purpose of this comparison is to verify the performance of the powered prosthesis compared with the passive prosthesis and if it has the potential to perform better.

For each group of comparisons, the results are to be evaluated according to two sets of data, which are the angle of the ankle and the moment in the ankle. The angle of the ankle evaluates the kinematic performance. The moment in the ankle evaluate the kinetic performance. The GRF and the power absorption or generation in the ankle are not critical design criteria for the design. The GRF evaluate the kinetic performance from another perspective and the power consumption evaluates the energy performance. They are found in Appendix. C.

6.3.1 Result Analysis between Trials Wearing Powered Prosthesis

Results Comparison

The ankle angle result of the three trials with wearing the powered prosthesis is shown in Fig. 6.3. It can be seen that the kinematics of the prosthetic ankle is consistent. The only relatively significant difference is that, for trial 3, during the loading response sub-phase, the prosthetic ankle is around 4 degree less plantar

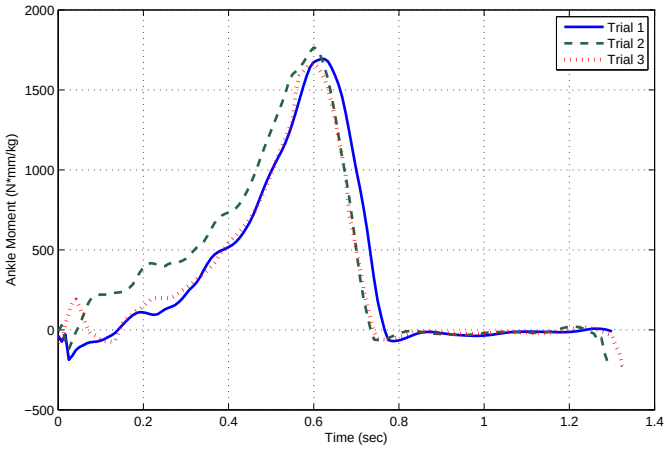

Figure 6.4: The Ankle Moment Comparison between the Three Trials of the Powered Prosthesis

flexion than the other two trials.

The prosthetic ankle moment comparison is shown in Fig. 6.4. The peak moment of these three trials are almost the same. The difference lies in that the moments in trial 2 starts to accumulate in the prosthesis earlier than trial 1 and trial 3; the moments in trial 1 releases a little later than trial 2 and trial 3.

Discussion

Fig. 6.3 shows that the prosthetic ankle performs consistently kinematically in the three trials. This consistency indicates that the ankle moment contributed by the angular displacement of the prosthetic ankle is consistent. As mentioned before in Chapter 3, the total prosthetic ankle moment is contributed by two sources: the angular displacement of the torsional spring and the motor. The moment provided by the spring is consistent between each trial, therefore, it can be concluded that the moment contributed by the motor is also consistent.

The consistency of the kinematic and kinetic data indicates that the prosthesis and its control system performs consistently between each trial. Therefore, the average of these three sets of data will be compared with the natural leg and the Winter's benchmark to see if the performance meets the design requirements.

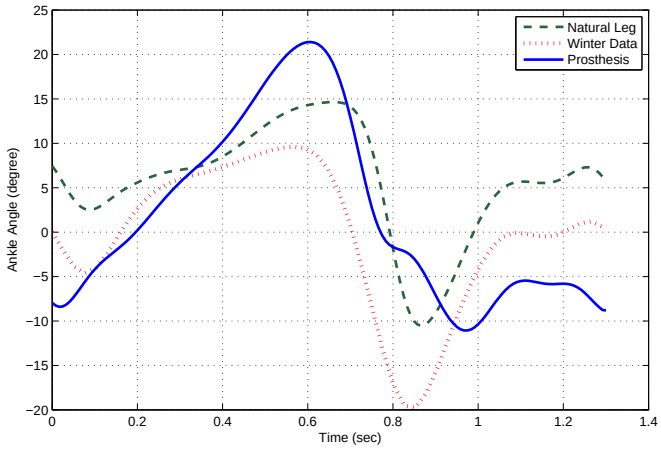

Figure 6.5: The Ankle Angle Comparison between the Powered Prosthesis, the Natural Leg and Winter's Data

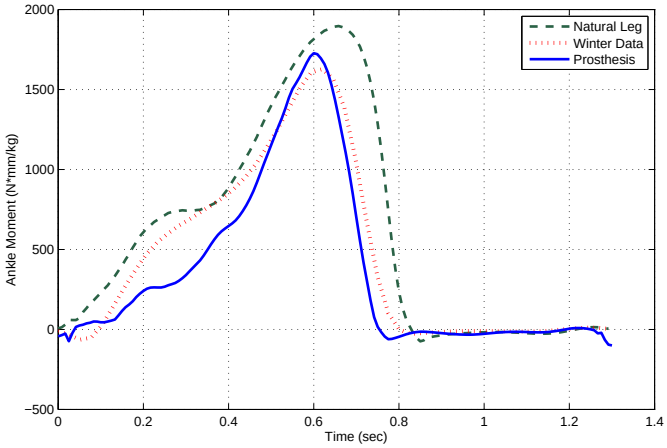

Figure 6.6: The Ankle Moment Comparison between the Powered Prosthesis, the Natural Leg and Winter's Data

6.3.2 Result Analysis between the Prosthesis, Natural Leg and Winter's Data

Results Comparison

The ankle angle data of the powered prosthesis testing, natural leg and the Winter's data is shown in Fig. 6.5. It can be seen that the powered prosthesis performs more dorsiflexion during the Stance Phase and performs more plantar flexion during the Swing Phase. The data between the amputee's natural leg and Winter's data is also different, with the amputee's natural leg performs more

dorsiflexion during the entire cycle of the gait.

The ankle moment comparison between the three is shown in Fig. 6.6. Comparing with the amputee's natural leg, the peak moment of the powered prosthesis is only around 5% smaller. Also, it can be seen that the push-off of the powered prosthesis is around 0.15 sec earlier than the natural leg.

Discussion

One major objective of the design of this powered prosthesis is to meet the reference ankle moment of Winter's benchmark, and thus an able-bodied person. It can be seen in Fig. 6.6 that this goal is achieved, with the moment in the powered prosthesis ankle is almost the same as the moment in the unaffected side.

The other objective of the design is that the powered prosthesis should go back to the neutral position during Swing Phase to get ready for the next heel strike. However, as shown in Fig. 6.5, the powered prosthesis performs around 9 degrees more plantar flexion at the end of the Swing Phase. This was also noticed by the amputee subject and the prosthetist during the testing. In the author's opinion, this is due to the limitation of the torsional spring and the mechanism designed. During the Swing Phase position control, the ankle joint was programmed to go to its maximum dorsiflexion position. Going further is going to break the torsional spring or the motor. This problem is going to be revisited in future work. Nevertheless, the amputee subject did state in the interview after the testing that he had enough foot clearance during the testing for the heel strike.

An explanation of why the push-off happens earlier in the powered prosthesis is due to the difference in the mechanism between the powered prosthesis and the passive one the amputee subject is used to. The amputee is still not familiar with the powered prosthesis.

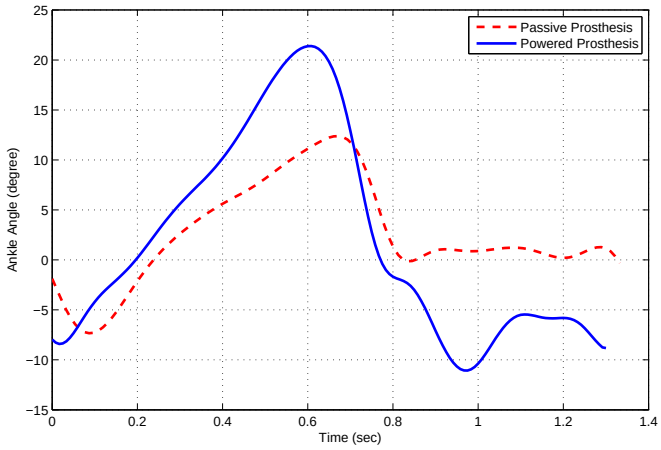

Figure 6.7: The Ankle Angle Comparison between the Powered Prosthesis and the Passive Prosthesis

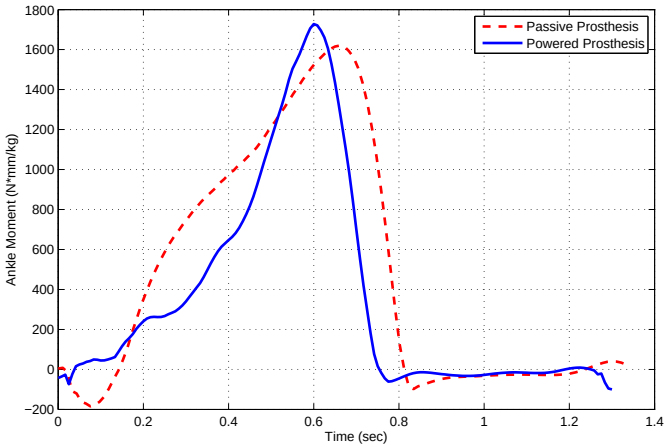

Figure 6.8: The Ankle Moment Comparison between the Powered Prosthesis and the Passive Prosthesis

6.3.3 Result Analysis between the Powered Prosthesis and the Passive Prosthesis

Results Comparison

The ankle angle result comparison between the powered prosthesis and the passive prosthesis is shown in Fig. 6.7. It can be noticed that similar as Fig. 6.5, the powered prosthesis performs more dorsiflexion during the Stance Phase and more plantar flexion at the end of the Swing Phase.

The ankle moment result comparison is shown in Fig. 6.8. It shows that the

peak moment before the push-off is around 10% larger in the powered prosthesis than the passive prosthesis. Similar to Fig. 6.6, the push-off happens earlier in the powered prosthesis than the passive one.

Discussion

The amputee testing subject informed that he has been using his passive prosthesis for several years, therefore it can be noticed that the kinematic performance of the passive prothesis is very similar to his natural leg as shown in Fig. 6.7. However, it can be noticed that the powered prosthesis generates around 10% more moment than the passive one during the Stance Phase, which will help with the amputee's push-off. This is also informed by the amputee subject in the interview after the testing that he did feel a "push-off" from the powered prosthesis when his prosthetic foot left the ground. This indicates again that the powered prosthesis achieves the goal of generating more energy in the ankle to help the amputee push-off.

Another advantage of the powered prosthesis is that the power it provides can be adjusted in the control system. It was mentioned in Chap 5 that even though with the existence of the energy loss inside the mechanism, the energy loss was not compensated in the control system in this first preliminary testing. If the power provided by the motor is magnified by a certain gain greater than one, the powered prosthesis is able to provide more moment to help with the push-off. This is going to be performed in future tests.

As shown in Fig. 6.8, the push-off happens earlier in the powered prosthesis than in the passive prosthesis. This is because of the same reason as discussed in Sec. 6.3.2. This problem will be addressed in future work.

6.4 Conclusion

A bench testing was first performed to verify that the control system's ability to meet the design requirements. Then, an amputee subject testing was performed to evaluate the design of the prosthesis. The testing method was described. The

results of the testing were illustrated and discussed. The results shows that the design objective of providing more moment than passive prostheses to help with the push-off is achieved. The results also indicates there are some problems with the powered prosthesis, such as more plantar flexion at the end of the Swing Phase and early push-off. These issues will be addressed in future work.

CHAPTER 7

Conclusion and Future Work

7.1 Conclusion

There are three major challenges in the ankle-foot prosthesis development. First, it is challenging to mimic the nonlinear behavior of a human ankle both in kinematics and kinetics. Second, it is challenging to match an able-bodied person's ankle moment magnitude with most of the ankle-foot prosthesis being passive and cannot actively provide power. Third, it is challenging to design a mechanism and control system that is small and light enough that its size and weight match that of an able-bodied person's lower limb.

In this project, the first challenge is met by using a very simple mechanism that includes a optimized four-bar mechanism and a torsional spring with optimized spring stiffness. A brushed DC motor is added to the mechanism to provide the extra required energy. One important assumption made for the design of the mechanism is that the amputee subject will perform the same kinematic angular displacement at the prosthetic ankle joint as an able-bodied person. The amputee subject testing results as shown in Fig. 6.5 and Fig. 6.6 show how similar it is between the reference nonlinear ankle profile and the performance of the powered prosthesis. The assumption and the design theory of the mechanism are both verified.

The objective of the control algorithm during the Stance Phase is to regulate the power of the motor so that the ankle moment matches Winter's reference. The amputee subject testing results in Fig. 6.8 shows that the motor did provide more moment than the passive prosthesis. Fig. 6.6 shows that the ankle moment in the powered prosthetic ankle is following the Winter's reference and was only slightly inferior comparing with the amputee's natural leg. Therefore, the second challenge

was met; the control program works correctly and the powered prosthesis did assist the amputee with the push-off.

The weight of the prosthesis designed in this project is 2.23kg, which is around the upper limit of the existing ankle-foot prosthesis. However, the amputee subject commented after the testing that he did not feel the powered prosthesis is heavier than his current passive prosthesis. This is consistent with one of the assumptions made during the mechanism design stage that the amputee will not fully feel the weight of the prosthesis if there is active power to assistant the amputee's push-off. Therefore, this assumption can serve as one of the fundamental assumptions in future work. However, a future prosthesis should still be designed as light as possible.

Because human gait can be divided into several states and each state has different dynamic feature and objectives, a multiple level control algorithm is more appropriate to control the powered below-knee prosthesis. As mentioned in Chap. 1, the Össur Proprio and the SPARKY from Arizona State University did not use multiple level control algorithms and only use simple position controllers. The MIT BioM and the Vanderbilt powered knee and ankle prosthesis have multiple level controllers which employ different type of controls for different states. This thesis is similar with the latter two prostheses in that it has two levels of controllers - a higher level FSC and lower level PID controllers. The control algorithm proposed in this thesis is different from the latter two in that it is a direct control of the moment and the angular position of the ankle, while the BioM and Vanderbilt prosthesis control the impedance of the prosthesis in order to reproduce ankle moment. The control algorithm employed in this thesis is simpler and more direct.

A DSP control board was used in this project as the processing unit of the control system. This is novel compared to the other powered lower limb prostheses, where PC 104 were normally used. The DSP control board has two major advantages over the other processors. First, it is faster in processing speed and much lighter. Second, the DSP microprocessor has many more peripherals which can be easily utilized such as GPIO and CAN communication. These two advantages bring great convenience in building the control system and realizing the

control algorithm. Also, the eZdsp F28335 control board, which is utilized in this project, can easily be programmed using MATLAB Simulink. The Simulink program can be automatically converted to executable code and downloaded to the DSP board. This brings an advantage over directly building the control program using C. In this author's opinion, the advantage of using DSP control board should be further investigated in the design of a future prosthesis.

Before CAN communication was selected, several communication methods were tried to communicate between the higher level master and the lower level slave, such as RS232 and PWM. CAN communication has several advantages over the others. First, it is a digital communication method, not an analog one; therefore, the command signal sent from the master to the slave is very accurate. Second, it has strong ability to resist the noise from the environment, which is important when during the amputee subject testing. Third, its communication speed is very fast. In this project, 500kHz was used. There is almost no lag in the communication between the master and the slave, which is a big advantage over the traditional communication method like PWM.

The approach to controller design used in this thesis is to use MATLAB Simulink to model the process and adjust the PID parameters of the controller. The traditional way is to derive the equations of motion, transfer functions, or state space functions explicitly, and then solve them either analytically or numerically. There are certain advantages and disadvantages of using this method compared with the traditional method. First, it is much easier to build and revise the model in computer software than having to change the derived the equations. Second, it is much easier to build and solve the nonlinear dynamic process in computer software. Since human gait is a highly nonlinear dynamic process and its operating point keeps shifting, if the traditional approach was used, linearization has to be done around several operating points and the equations have to be solved several times. In the proposed approach, the computer software is able to solve these nonlinear equations in the background quickly, thus saving a lot of effort and time. Third, the dynamic process can be animated and plotted conveniently so the users can have a intuitive feeling of how the dynamic process looks like. The disadvantages is that

the equations of motion are not shown explicitly in the computer software so that the user has to trust the results of the simulation and it is very difficult for the users to verify the results.

7.2 Future Work

The amputee subject testing showed that the design theory of the control algorithm were proved to be successful, even though the efficiency needs to be significantly improved. Based on the design of this thesis, both the higher level and lower level controllers can be improved to the next level. The mechanism design can be also improved. The future work should focus on one or several of the outlined aspects.

7.2.1 Improve the Efficiency

As described in previous chapters, when the brushed DC motor is running at lower speed, the efficiency of the motor drops to a very low level. Also the energy loss in the mechanism is significant. Therefore, increasing the overall efficiency of the prosthesis should be emphasized in the future. The mechanism could be re-designed to have better efficiency, better lubrication could be used, etc. If the efficiency of the prosthesis can be raised significantly, smaller battery pack can be used in future testing and the control system can become much lighter.

7.2.2 Reselection of the Motor

The underdesigned motor can be one reason which cause the failure to achieve the swing phase control objective. The selection of the motor should be revisited. A better power rated motor should be reselected. The other type of motors could be also selected to raise the efficiency of the motor. A brushless DC motor or a servo motor should be tested.

7.2.3 More Sophisticated Higher Level Control Algorithm

There are two directions the higher level FSC algorithm could be improved in two ways. First, in the current level walking FSC, the control schematic could be made to consider more normal or abnormal situations so that it is more robust. This prosthesis in the future should be able to walk in different patterns. More control patterns could be added into the FSC algorithm, such as walking ascent, walking descent, running or walking backwards control. If a complete set of FSC can be developed, the prosthesis will become more robust and be able to satisfy needs for all day usage.

7.2.4 More Advanced Lower Level Controller

PID controllers are currently used for lower level control. It is simple and easy to implement. However, the ankle dynamics of the human gait is nonlinear. In addition, if more gait patterns are programmed into the higher level FSC in the future, one single set of PID parameters probably will not satisfy the need. Therefore, a more advanced control algorithm could be used for the lower level control in the future, such as nonlinear controller, adaptive control and some other control algorithm which could make the lower level control work more precisely and adaptively.

7.2.5 Redesign the Portable Platform

The entire control system components are currently laid out and place on a backpack. However, this backpack is bulky and heavy considering everyday use. During the amputee subject testing, the subject had to wear this backpack while walking on the prosthesis which already showed some inconvenience. For the next generation of the prosthesis, the portable platform needs to be redesigned so that it becomes smaller and lighter. Another form of the backpack should be considered as well, such as in the form of a belt or a system which could be integrated with the prosthesis.

REFERENCES

[1] Proprio Foot with Evo, Technical Manual, 2010.

[2] R.D. Bellman, M.A. Holgate, and T.G. Sugar. SPARKy 3: Design of an active robotic ankle prosthesis with two actuated degrees of freedome using regnerative kinetics. In *Proceedings of 2nd Biennial IEEE/RAS-EMBS International Conference on Biomedical Robotics and Biomechatronics*, pages 511–516, Scottsdale, AZ, October 2008.

[3] J.K. Hitt, T.S. Sugar, M. Hogate, and R. Bellman. An active foot-ankle prosthesis with biomechanical energy regeneration. *Journal of Medical Devices*, 4(1), March 2010.

[4] Huseyin Atakan Varol, Frank Sup, and Michael Goldfarb. Multiclass real-time intent recognition of a powered lower limb prosthesis. *IEEE Transactions on Biomedical Engineering*, 57(3):542–551, March 2010.

[5] Frank Sup, Huseyin Atakan Varol, Jason Mitchell, Thomas. J Withrow, and Michael Goldfarb. Preliminary evaluations of a self-contained anthropomorphic transemoral prosthesis. *IEEE/ASME Transactions on Mechatronics*, 14(6):667–676, December 2009.

[6] S.K.Au. *Powered ankle-foot prosthesis for the improvement of amputee walking economy*. Ph.D dissertation, Massachusetts Institute of Technology, Cambridge, MA, June 2007.

[7] David.A. Winter. *Biomechanics and motor control of human movement*. Wiley-Interscience, 1990.

[8] D.Smith. Transtibial amputations: Successes and challenges. *inMotion*, 13(4):57–63, July/August 2003.

[9] T.R. Dillingham, L.E. Pezzin, and E.J. MacKenzie. Limb amputation and lmb deficiency: Epidemiology and recent trends in the united states. *Southern Medical Journal*, 95(8), August 2002.

[10] A.H. Hansen, D.S. Childress, S.C. Miff, S.A. Gard, and K.P. Mesplay. The human ankle during walking: implications for design of biomimetic ankle prostheses. *Journal of Biomechanics*, 37:1467–1474, 2004.

[11] Jacquelin Perry and Judith Burnfield. *Gait analysis: Normal and pathological function*. Slack Incoporated, 2010.

[12] Leslie Torburn, Christoper M. Powers, Robert Guiterrez, and Jacquelin Perry. Energy expenditure during ambulation in dysvascular and traumatic below-knee amputees; a comparison of five prosthetic feet. *Journal of Rehabilitation Research and Development*, 32(2):111–119, May 1995.

[13] Bryan.J. Bergelin. Design of a transtibial prosthesis utilizing active and passive components in conjunction with a four-bar mechanism. M.S thesis, Marquette University, Milwaukee, WI, August 2010.

[14] J.K. Hitt, T.S. Sugar, M. Hogate, R. Bellman, and K. Hollander. Robotic transtibial prosthesis with biomechanical energy regeneration. *Industrial Robot: An International Journal*, 36(5), 2009.

[15] J.K. Hitt, R. Bellman, T.G. Holgate, M. Sugar, and K.W. Hollander. The SPARKY (spring ankle with regenerative kinetics) project: Design and analysis of a robotic transtibial prosthesis with regenerative kinetics. In *Proceedings of the 2007 ASME IDETC/CIE*, September 2007. Paper Number DETC2007-34512.

[16] J.K. Hitt, A. Oymagil, T. Sugar, K. Hollander, A. Boehler, and J. Fleeger. Dynamically controlled ankle-foot orthosis with regenerative kinetics: Incrementally attaining user portability. In *Proceedings of the 2007 IEEE International Conference on Robotics and Automation*, pages 1541–6, Roma, 2007.

[17] M. Whittle. *Gait Analysis: An Introduction*. Oxford, 1996.

[18] M.A. Holgate, A.W. Bohler, and T.G. Sugar. Control algorithms for ankle robots: A reflection on the state-of-the-art and presentation of two novel algorithms. In *Proceedings of 2nd Biennial IEEE/RAS-EMBS International Conference on Biomedical Robotics and Biomechatronics*, pages 97–102, Scottsdale, AZ, October 2008.

[19] M.A. Holgate, T.G. Sugar, and A.W. Bohler. A novel control algorithm for wearable robotics using phase plane invariants. In *Proceedings of 2009 IEEE International Conference on Robotics and Automation*, pages 3845–3850, Kobe, Japan, May 2009.

[20] Frank Sup, Amit Bohara, and Michael Goldfarb. Design and control of a powered transfemoral prosthesis. *The International Journal of Robotics Research*, 27(2):263–273, February 2008.

[21] Samuel.K. Au and Hugh Herr. Powered ankle-foot prosthesis: The importance of series and parallel elasticity. *IEEE Robotics and Automation Magzine*, 15(3):51–66, February 2008.

[22] Samuel.K. Au, Jeff Weber, and Hugh Herr. Powered ankle-foot prosthesis improves walking metabolic economy. *IEEE Transaction on Robotics*, 25(1):52–59, September 2009.

[23] Michael.F Eilenberg, Hartmut Geyer, and Hugh Herr. Control of a powered ankle-foot prosthesis based on a neuromuscular model. *IEEE Transactions on Neural Systems and Rehabilitation Engineering*, 18(2):164–173, April 2010.

[24] Javier.O. Mattos, Evan.D. Kane, and Philip.A. Voglewede. Active component lower limb prosthetic device research: Concept and design. In *Proceedings of ASME 2007 International Design Engineering Technical Conferences and Computer and Information in Engineering Conference*, pages 607–613, Las Vegas, NV, September 2007.

[25] Bryan.J. Bergelin, Joavier.O. Mattos, Joseph.G. Wells, and Philip.A. Voglewede. Concept through preliminary bench testing of a powered lower limb prosthetic device. *Journal of Mechanisms and Robotics*, 2(4), November 2010.

[26] Robert Norton. *Design of Machinery*. McGraw-Hill, 2003.

[27] Texas Instruments. *TMS320F28335 Digital Signal Controllers Data Manual*, March 2011.

[28] CGI, INC., 3400 Arrowhead Drive, Carson City, NV, 89706. *CGI Technical Catalog*, 2006.

[29] http://www.mathworks.com/products/simmechanics/.

APPENDIX A

Kinematics Derivation of the Four-Bar Mechanism

Figure. A.1 shows a sketch of the four-bar mechanism. For the convenience of the calculation, define θ_2, θ_3 and θ_4 as shown in Fig. A.1. $\frac{\dot{\theta}}{\dot{\phi}}$ can be expressed as a function of $\frac{\dot{\theta_3}}{\dot{\theta_2}}$ as shown in Eqn. A.1:

$$\frac{\dot{\theta}}{\dot{\phi}} = \frac{1}{1 - \frac{\dot{\theta_3}}{\dot{\theta_2}}} \tag{A.1}$$

Therefore, if $\frac{\dot{\theta_3}}{\dot{\theta_2}}$ is obtained, the value of $\frac{\dot{\theta}}{\dot{\phi}}$ can be obtained. As shown in Fig. A.1, the variables and parameters that are known are the length of each bar l_0, l_1, l_2 and l_3, the angle θ_3 and angular velocity $\dot{\theta}_3$. The value $\frac{\dot{\theta_3}}{\dot{\theta_2}}$ needs to be determined.

Define the coordinate system XYZ as shown in Fig. A.1. Consider each link as a vector whose direction is indicated by the arrowheads shown in Fig. A.1. The

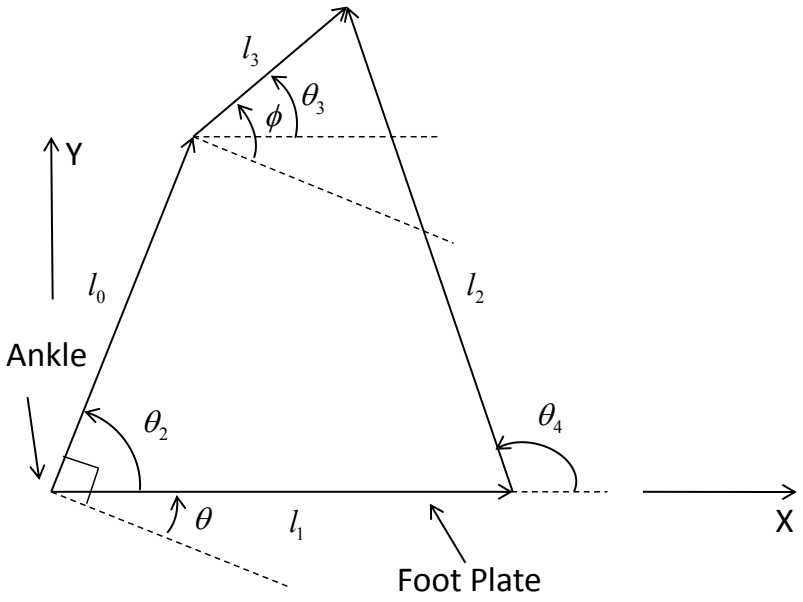

Figure A.1: The Sketch of the Four-Bar Mechanism Kinematics

summation of the linkage vectors should be zero. Therefore:

$$\vec{l_0} + \vec{l_3} - \vec{l_1} - \vec{l_2} = 0 \tag{A.2}$$

Using complex number notation to express these vectors, Eqn. A.2 can be expressed as:

$$l_0 e^{j\theta_2} + l_3 e^{j\theta_3} - l_1 e^{j\theta_1} - l_2 e^{j\theta_4} = 0 \tag{A.3}$$

where j is the complex number. Taking derivative of Eqn. A.3, it becomes:

$$jl_0 e^{j\theta_2}\frac{d\theta_2}{dt} + jl_3 e^{j\theta_3}\frac{d\theta_3}{dt} - jl_1 e^{j\theta_1}\frac{d\theta_1}{dt} - jl_2 e^{j\theta_4}\frac{d\theta_4}{dt} = 0 \tag{A.4}$$

According to Fig. A.1, l_1 is a link which is fixed to the ground. Therefore, $\dot{\theta_1}$ is always zero and the third term in Eqn. A.4 can be ignored. In complex number notation, $e^{j\theta}$ can be expressed as:

$$e^{j\theta} = \cos\theta + j\sin\theta \tag{A.5}$$

Substituting Eqn. A.5 into Eqn. A.4, collecting the terms according to the real parts and the imaginary parts, Eqn. A.4 becomes:

$$-l_0\dot{\theta_2}\sin\theta_2 - l_3\dot{\theta_3}\sin\theta_3 + l_2\dot{\theta_4}\sin\theta_4 + j(l_0\dot{\theta_2}\cos\theta_2 + l_3\dot{\theta_3}\cos\theta_3 - l_2\dot{\theta_4}\cos\theta_4) = 0 \tag{A.6}$$

To make the left side of Eqn. A.6 zero, both the real and imaginary parts need to be zero. Therefore:

$$\begin{aligned} -l_0\dot{\theta_2}\sin\theta_2 - l_3\dot{\theta_3}\sin\theta_3 + l_2\dot{\theta_4}\sin\theta_4 &= 0 \\ l_0\dot{\theta_2}\cos\theta_2 + l_3\dot{\theta_3}\cos\theta_3 - l_2\dot{\theta_4}\cos\theta_4 &= 0 \end{aligned} \tag{A.7}$$

Combining the equations in Eqn. A.7 and eliminating the term θ_4, the following equation can be obtained:

$$l_0\dot{\theta_2}\sin(\theta_4 - \theta_2) + l_3\dot{\theta_3}\sin(\theta_4 - \theta_3) = 0 \tag{A.8}$$

Reorganizing Eqn. A.8 one can get the desired form:

$$\frac{\dot{\theta_3}}{\dot{\theta_2}} = \frac{l_0 \sin(\theta_2 - \theta_4)}{l_3 \sin(\theta_4 - \theta_3)} \tag{A.9}$$

In Eqn. A.9, the terms l_0, l_3 and θ_3 are known. θ_2 and θ_4 are not known yet. However, they are dependent on the value of θ_3. Therefore, they can be expressed by a function of θ_3. Separating Eqn. A.2 into X and Y components, the following equations can be obtained:

$$\begin{aligned} XAxis : l_2 \cos\theta_4 &= l_3 \cos\theta_3 + l_0 \cos\theta_2 - l_1 \\ YAxis : l_2 \sin\theta_4 &= l_3 \sin\theta_3 + l_0 \sin\theta_2 \end{aligned} \tag{A.10}$$

Squaring both equations in Eqn. A.10 and combining them together, they are transformed to:

$$-\cos\theta_2 - \frac{l_3}{l_0}\cos\theta_3 + \frac{l_3}{l_1}\cos(\theta_2 - \theta_3) + \frac{l_0^2 + l_1^2 - l_2^2 + l_3^2}{2l_0 l_1} = 0 \tag{A.11}$$

To simplify the expression of Eqn. A.11, define:

$$\begin{aligned} K_1 &= \frac{l_3}{l_0} \\ K_2 &= \frac{l_3}{l_1} \\ K_3 &= \frac{l_0^2 + l_1^2 - l_2^2 + l_3^2}{2l_0 l_1} \end{aligned} \tag{A.12}$$

Substituting Eqn. A.12 into Eqn. A.11, Eqn. A.11 becomes:

$$(K_2 \cos\theta_3 - 1)\cos\theta_2 + K_2 \sin\theta_3 \sin\theta_2 - K_2 \cos\theta_3 + K_3 = 0 \tag{A.13}$$

Using the trigonometric functions, $\cos\theta_2$ and $\sin\theta_2$ can be expressed as a function of

$\tan\theta_2$. Therefore, the following equations can be obtained:

$$(K_3 - K_1\cos\theta_3 + 2 - K_2\cos\theta_3)\tan^2\left(\frac{\theta_2}{2}\right) +$$
$$2K_2\sin\theta_3\tan\left(\frac{\theta_2}{2}\right) + (K_2\cos\theta_3 - 1 + K_3 - K_1\cos\theta_3) = 0 \quad \text{(A.14)}$$

To simplify the expression of Eqn. A.14, define:

$$\begin{aligned} A &= K_3 - K_1\cos\theta_3 + 1 - K_2\cos\theta_3 \\ B &= 2K_2\sin\theta_3 \\ C &= K_2\cos\theta_3 - 1 + K_3 - K_1\cos\theta_3 \end{aligned} \quad \text{(A.15)}$$

Solving Eqn. A.14, the value of θ_2 can be expressed as a function of θ_3 as:

$$\theta_2 = 2\arctan\left[\frac{-B + \sqrt{B^2 - 4AC}}{2A}\right] \quad \text{(A.16)}$$

Repeating the same procedure from Eqn. A.10 to Eqn. A.16 for θ_4, θ_4 can be also expressed as a function of θ_3 which is:

$$\theta_4 = 2\arctan\left[\frac{-E + \sqrt{E^2 - 4DF}}{2D}\right] \quad \text{(A.17)}$$

where D, E, F are:

$$\begin{aligned} D &= K_2\cos\theta_3 - 1 + K_5 - K_4\cos\theta_3 \\ E &= -2K_2\sin\theta_3 \\ F &= 1 - K_2\cos\theta_3 + K_5 - K_4\cos\theta_3 \end{aligned} \quad \text{(A.18)}$$

where K_4 and K_5 are:

$$\begin{aligned} K_4 &= \frac{l_3}{l_2} \\ K_5 &= \frac{l_1^2 + l_2^2 + l_3^3 - l_0^2}{2l_1l_2} \end{aligned} \quad \text{(A.19)}$$

Using Eqn. A.16 and Eqn. A.17, θ_2 and θ_4 can be expressed as a function of θ_3. Therefore, $\frac{\dot{\theta}_3}{\dot{\theta}_2}$ can be calculated using Eqn. A.9. The value of $\frac{\dot{\theta}}{\dot{\phi}}$ can be then calculated using Eqn. A.1. Therefore, how much moment needs to be generated from the motor can be obtained in real time using Eqn. 3.2.

APPENDIX B

Simulink and Stateflow Control Program

The overall control program built in Simulink and its Stateflow toolbox is shown in Fig. B.1. There are four major components in this program. The first is the higher level control program which is shown as the orange Stateflow block. The second is the lower level control program which is shown as the green Stateflow block. The third is the FSR sensors feedback which are shown as the four purple subsystem blocks.

The fourth are the two light blue CAN communication blocks. The one on the top is CAN receive which feedback the encoder position and velocity, current running through the motor armature and other information from the EPOS2 to the DSP. The one at the bottom is the CAN transmit which sends higher level FSC commands to the lower level EPOS2 motor controller. The higher level control program built using Stateflow toolbox is shown in Fig. B.2.

The lower level control algorithm also built in Stateflow toolbox can be divided into PI moment control and PID position control. The program of the PI moment controller is shown in Fig. B.3. The MATLAB function embedded in the Stateflow program uses the reference input and the feedback of the angular position of the torsional spring to calculate the moment control input into the PID controller.

The lower level PID position control program is shown in Fig. B.4.

The Simulink program of the FSR sensors which are inside the orange subsystems is shown in Fig. B.5.

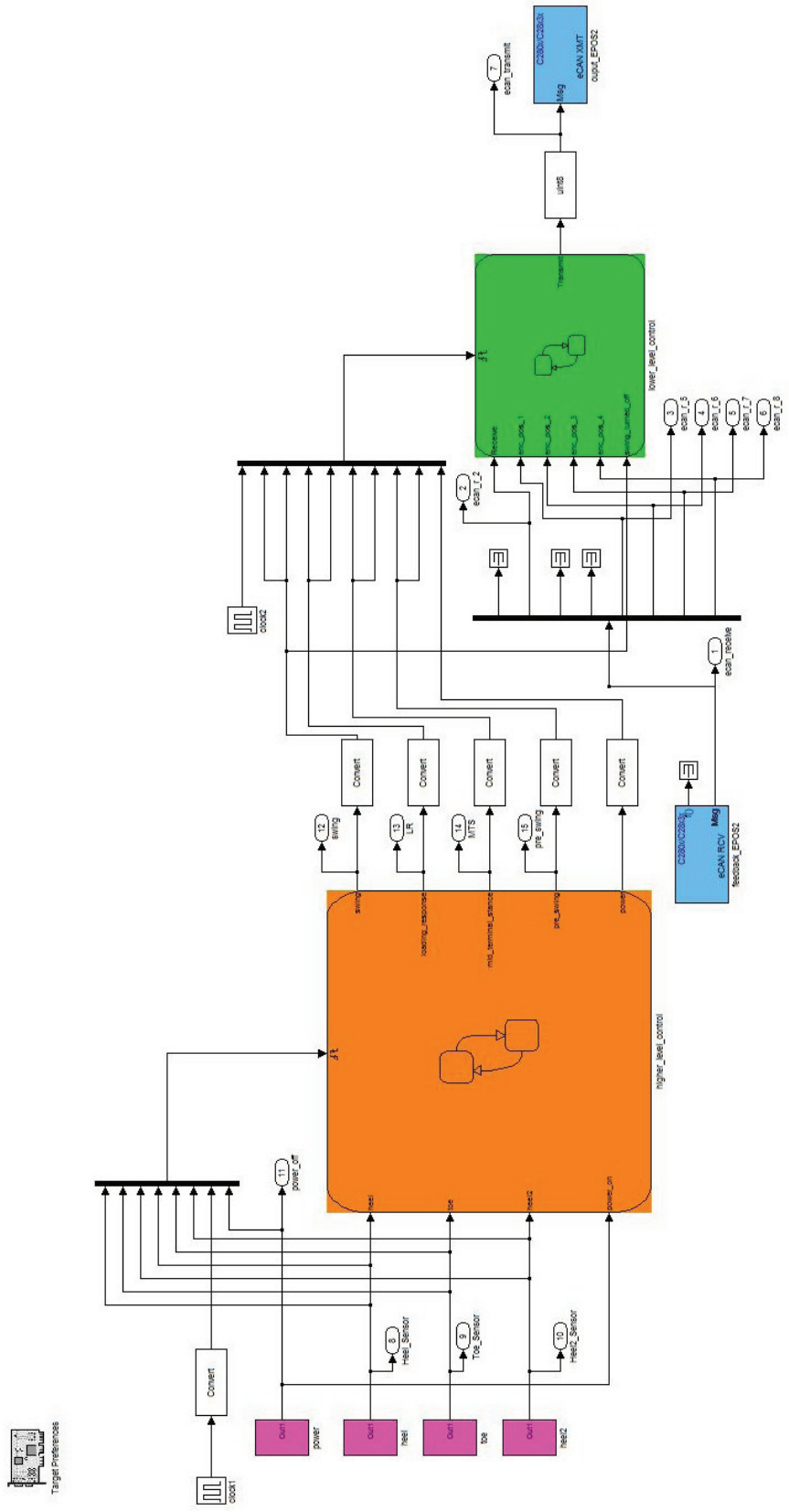

Figure B.1: Overall Control Program Built in Simulink and Stateflow Toolbox

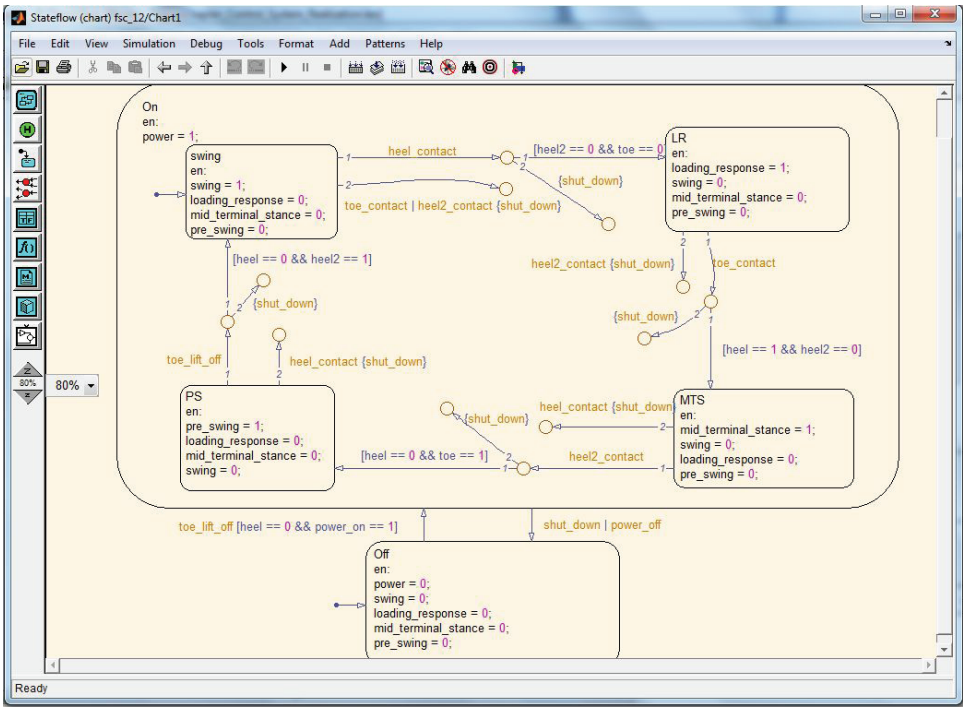

Figure B.2: Higher Level Control Program Using Stateflow Toolbox

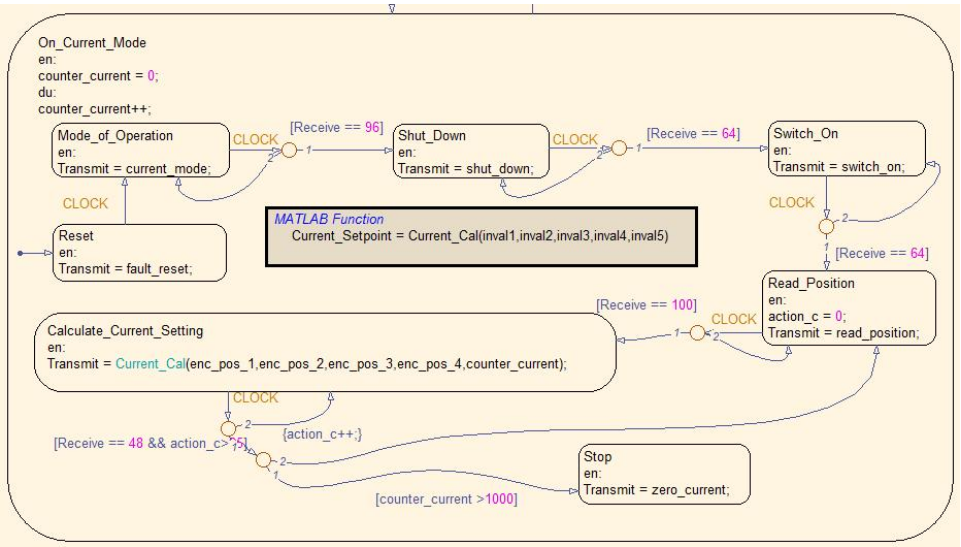

Figure B.3: Lower Level PI Moment Control Program

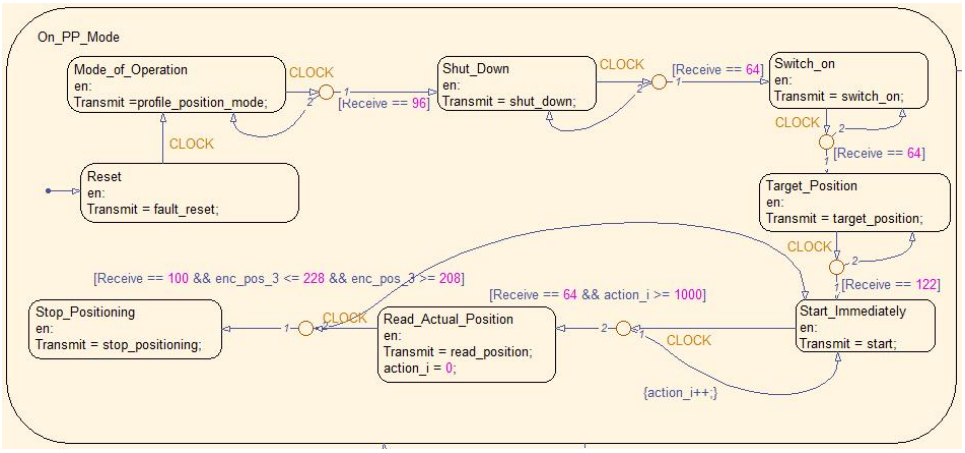

Figure B.4: Lower Level PID Position Control Program

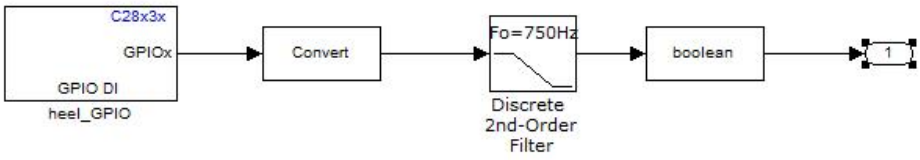

Figure B.5: FSR Simulink Subsystem

APPENDIX C

Amputee Subject Testing Data

Figure. C.1 and Fig. C.2 show the comparison of the GRF and the power generation or consumption between the three trials when the amputee was wearing the powered prosthesis. Fig. C.3 and Fig. C.4 show the comparison of the GRF and the power generation or consumption between the powered prosthesis, natural leg and the Winter's reference data. Fig. C.5 and Fig. C.6 show the comparison of the GRF and the power generation or consumption between the powered prosthesis and the amputee's original passive prosthesis.

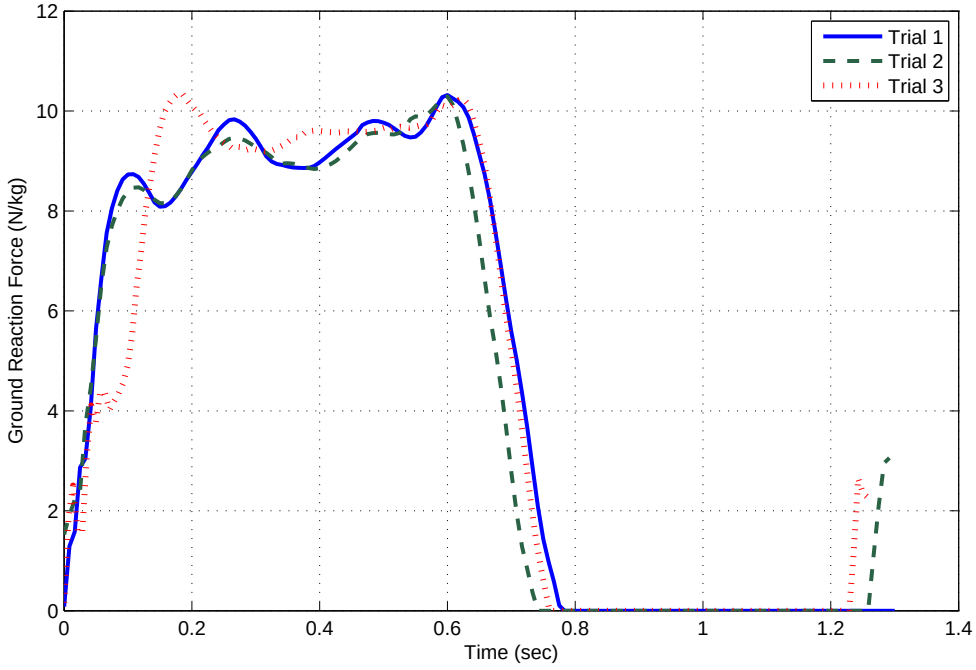

Figure C.1: The GRF Comparison between the Three Trials of the Powered Prosthesis

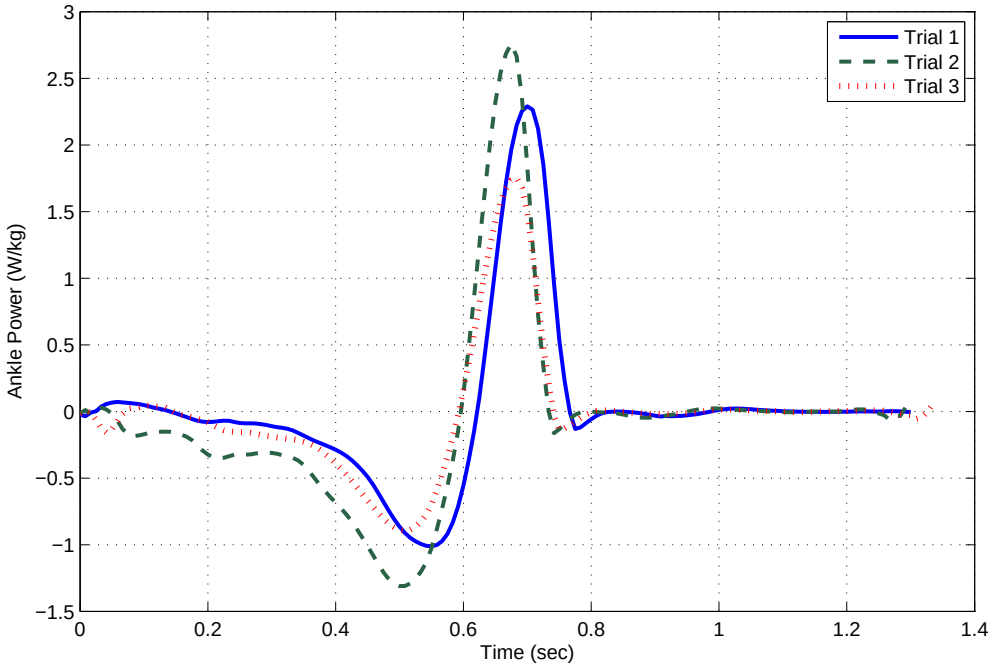

Figure C.2: The Ankle Power Comparison between the Three Trials of the Powered Prosthesis

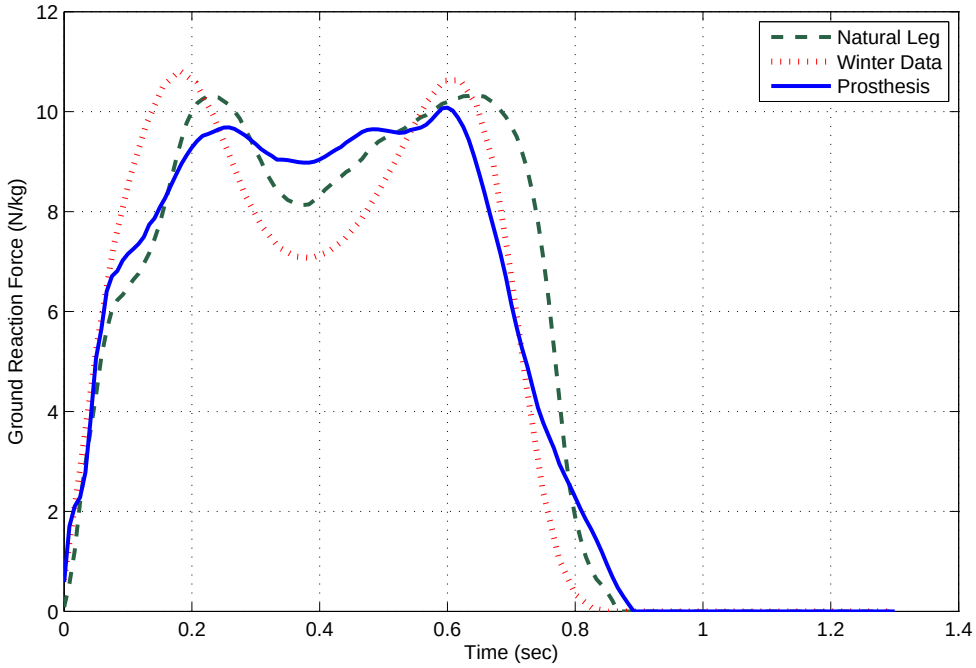

Figure C.3: The GRF Comparison between the Powered Prosthesis, the Natural Leg and Winter's Data

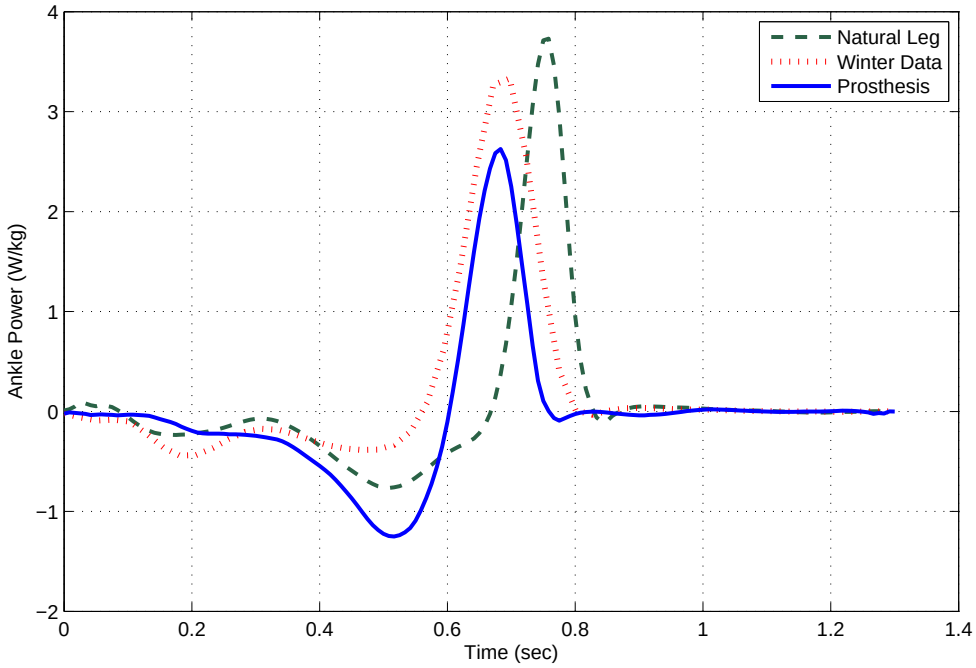

Figure C.4: The Ankle Power Comparison between the Powered Prosthesis, the Natural Leg and Winter's Data

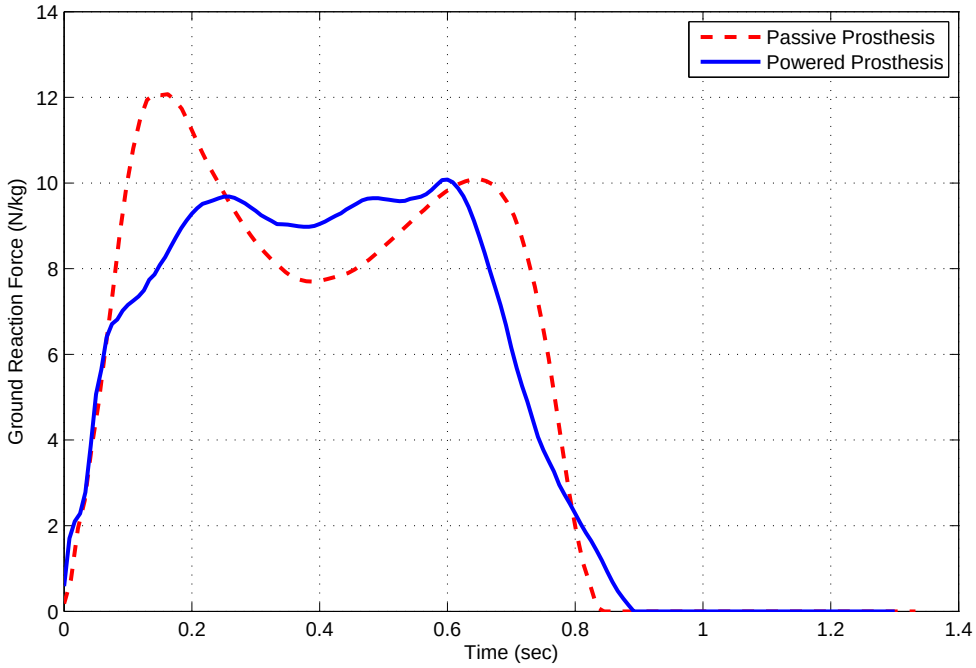

Figure C.5: The GRF Comparison between the Powered Prosthesis and the Passive Prosthesis

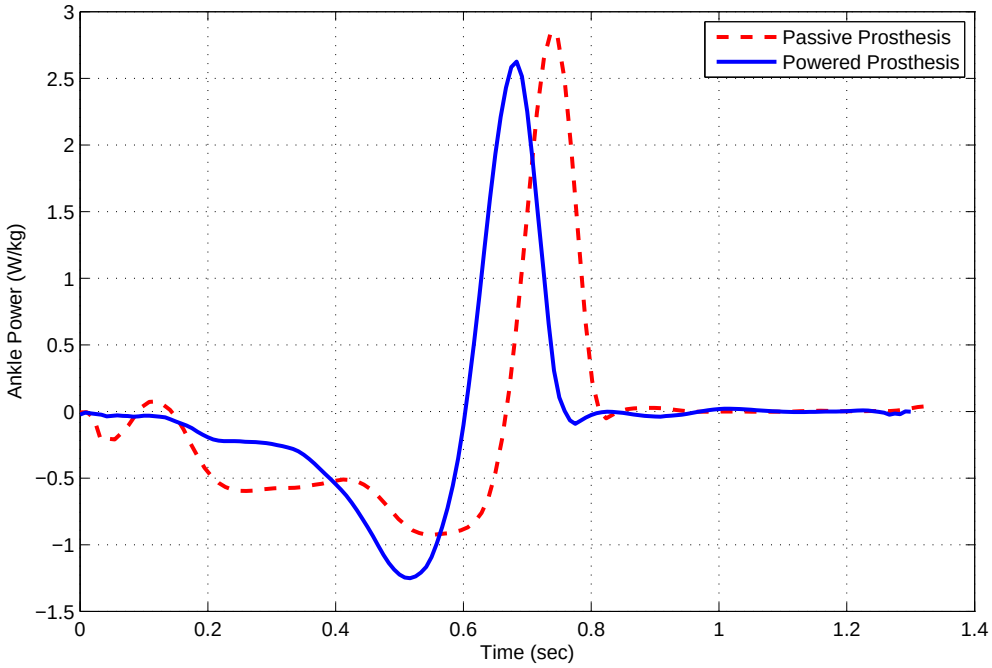

Figure C.6: The Ankle Power Comparison between the Powered Prosthesis and the Passive Prosthesis